Bulletin of Mathematical Biology (1999) **61**, 303–339
Article No. bulm.1998.0082
Available online at http://www.idealibrary.com on IDEAL

Zooplankton Mortality and the Dynamical Behaviour of Plankton Population Models

ANDREW M. EDWARDS*
Biology Department,
Woods Hole Oceanographic Institution,
Woods Hole, MA 02543, U.S.A.

Department of Applied Mathematical Studies and Centre for Nonlinear Studies, University of Leeds, Leeds LS2 9JT, U.K.
E-mail: andy@caligo.bio.dfo.ca

JOHN BRINDLEY
Department of Applied Mathematical Studies
and Centre for Nonlinear Studies,
University of Leeds,
Leeds LS2 9JT, U.K.

We investigate the dynamical behaviour of a simple plankton population model, which explicitly simulates the concentrations of nutrient, phytoplankton and zooplankton in the oceanic mixed layer. The model consists of three coupled ordinary differential equations. We use analytical and numerical techniques, focusing on the existence and nature of steady states and unforced oscillations (limit cycles) of the system. The oscillations arise from Hopf bifurcations, which are traced as each parameter in the model is varied across a realistic range. The resulting bifurcation diagrams are compared with those from our previous work, where zooplankton mortality was simulated by a quadratic function—here we use a linear function, to represent alternative ecological assumptions. Oscillations occur across broader ranges of parameters for the linear mortality function than for the quadratic one, although the two sets of bifurcation diagrams show similar qualitative characteristics. The choice of zooplankton mortality function, or closure term, is an area of current interest in the modelling community, and we relate our results to simulations of other models.

1. INTRODUCTION

The sunlit surface waters of the world's oceans are populated by tiny plankton. *Plankton* is a general term used to describe freely-floating and weakly-swimming marine and freshwater organisms. It comes from a Greek word ($\pi\lambda\alpha\nu\kappa\tau o\varsigma$) meaning wandering or drifting, and was introduced by the German scientist Victor Hensen in 1887 (Thurman, 1997). At around the same time, the French mathematician Henri

*Author to whom correspondence should be addressed: Biological Oceanography Division, Bedford Institute of Oceanography, B240, Dartmouth, Nova Scotia, Canada B2Y 4A2.

0092-8240/99/020303 + 37 $30.00/0

Poincaré was laying down the foundations for a geometric approach to analysing the dynamics of nonlinear systems. In this paper we invoke the theory of dynamical systems that has arisen from Poincaré's pioneering work to investigate the behaviour of plankton population models.

Plankton may be broadly divided into two groups. Phytoplankton are the plants and are mostly microscopic in size and unicellular; they are consumed by zooplankton, the animals, which in turn are eaten by larger organisms. In addition to their role at the base of the food chain, phytoplankton influence the global carbon cycle, with consequences for climate change that are at present undetermined (Denman *et al.*, 1996). Direct measurement of plankton biomass is difficult and expensive, and so the modelling of plankton populations is an essential tool to improve our understanding of the physical and biological processes which affect the population dynamics. Results from simple models can indicate to researchers dealing with large models which aspects of model formulation are most crucial in determining the output. In particular, the works of Evans and Parslow (1985) and Steele and Henderson (1992) concerning simple models are often considered when larger simulation models, such as the seven-component Fasham (1993) model, are being formulated.

Steele and Henderson (1992) demonstrated that the choice of functional form and parameter values used to model zooplankton mortality can have a major influence on the dynamics of simple models. They found that, for their particular parameter values, limit cycle behaviour (unforced oscillations) which occurred when using a linear zooplankton mortality term did not occur when using a quadratic term. In contrast to this, we have shown (Edwards and Brindley, 1996) that limit cycle behaviour occurs over broad ranges of parameter values when a quadratic term is used for zooplankton mortality. The model that we examined was based on the nutrient-phytoplankton-zooplankton (*NPZ*) model of Steele and Henderson (1981), extended in the manner of Steele and Henderson (1993). Here we build upon our earlier work by replacing the quadratic zooplankton mortality term with a linear term, to investigate further the importance of this (sometimes arbitrary) choice of function.

Ryabchenko *et al.* (1997) have investigated short-term oscillations which can arise in phytoplankton data (Williams, 1988) and in the output of large ecosystem models (Fasham, 1993). Such oscillations occur some years in the North Atlantic Ocean during the summer, and have a period of the order of 1 month. For the remainder of the year such short-term oscillations do not occur. This suggests that the seasonal forcing of some of the parameters may be taking the system from a region of parameter space where the unforced system would be attracted to a stable steady state, into a region during the summer months where the unforced system would exhibit stable oscillatory behaviour. In this paper we compute such regions of oscillatory behaviour for our model, as defined by the location of Hopf bifurcations. Yool (1998) has also investigated such oscillations, and we discuss his results in the context of our work in the Discussion section.

In the freshwater context, McCauley and Murdoch (1987) analysed data from over 30 studies in 12 countries which reported the seasonal dynamics of the crus-

tacean zooplankton *Daphnia* and their phytoplankton prey across a wide variety of habitats. Excluding data from the spring rise and fall in populations, which is driven by external environmental factors, they found internally-driven cycles of the populations in 15 cases. The means of the periods of the cycles range from 25–54 days, and the cycles were claimed to be internally driven because of similarities with laboratory populations, from which external influences are excluded. We find cycles of such periods in our model in this paper; the model is not forced by any external factors, and so the cycles must be internally driven. Although the work of McCauley and Murdoch (1987) is concerned with freshwater rather than marine plankton, we mention it here as evidence that the cycling of populations does occur; in the ocean, the more turbulent environment could act to conceal any clear signal identifying such cycles.

Our model has similarities with other food-chain models [e.g., Hastings and Powell (1991)], and consequently our results may be relevant to a wider spectrum of population models, not just those concerned with plankton. Furthermore, the two-component phytoplankton-zooplankton model of Steele and Henderson (1981) has since been used as a fish model (in which the variables represent fish populations rather than plankton populations) by Collie and Spencer (1994) to model fluctuations in abundances of Pacific hake (predator) and Pacific herring (prey) off the west coast of Vancouver Island, British Columbia. Thus even 'plankton' models are applied to other populations.

We describe the model and parameter ranges in Section 2. The model differs from that of Edwards and Brindley (1996) in that the quadratic term for zooplankton mortality, dZ^2, in the equations is replaced by the linear form qZ, where d and q are the mortality rates (with different definitions), and Z is zooplankton concentration. The zooplankton mortality term is called the 'closure term' by Steele and Henderson (1992) because it closes the model at the top trophic level, and it primarily represents consumption of the zooplankton by higher predators. Natural mortality is usually implicitly assumed by modellers to be included in the closure term. The quadratic and linear forms for the closure term represent different ecological assumptions—for dZ^2, the specific (per capita) rate is dZ, which assumes that higher predators have a biomass proportional to their prey, whereas the linear qZ function assumes a constant specific higher-predation rate, q. The linear form is often used due to it being the most simple form, and because of the lack of data that would strongly support an alternative form. Steele and Henderson (1992), when discussing the use of the linear form, said that 'There can be a strong empirical basis for this approach if nothing is known (or can be known) about the actual ecological context'.

In Section 3 we analyse the system, and derive far more information about the location and stability of the steady states algebraically, without having to invoke any specific values of the parameters, than we could for the quadratic case in Edwards and Brindley (1996). We show that there is at most one steady state with strictly positive values of nutrient, phytoplankton and zooplankton, and we

determine conditions for its stability. The absence of coexisting strictly positive steady states means that the hysteresis behaviour found by Edwards and Brindley (1996) for the quadratic case cannot occur.

We then perform a numerical investigation into the dynamical behaviour of the system using q, the linear zooplankton mortality rate, as the primary bifurcation parameter. This parameter is a particularly difficult parameter to measure; the equivalent quadratic rate, d, was varied by Steele and Henderson (1981), and was consequently used by Edwards and Brindley (1996) as a bifurcation parameter. In Section 4, we firstly plot the trajectory of the system when all the parameters are set at their default values, and then show that at an increased value of q the asymptotic behaviour of the system is qualitatively different, exhibiting oscillations rather than settling down to a steady state. This difference is explained by the one-parameter bifurcation diagrams constructed in Section 5, where only q is varied. The diagrams indicate values of q at which Hopf bifurcations occur. Hopf bifurcations, by definition, demarcate the values of q for which the steady state is stable or unstable—limit cycles (usually) occur where the steady state is unstable. In Section 6, each of the other parameters in the model is varied in turn, together with q, to produce two-parameter bifurcation diagrams which demonstrate how the region of limit cycles changes as the other parameters are varied. In Section 7 we construct period–contour diagrams, illustrating how the period of the oscillations changes as each parameter is varied. We discuss our results in Section 8, and in the Appendix present the method used for computing the period–contour diagrams of Section 7.

The numerical analysis has involved a combination of the numerical bifurcation packages AUTO (Doedel *et al.*, 1994) and LOCBIF (Khibnik *et al.*, 1992, 1993) to examine the bifurcations, with PLAUT and IDL used to produced many of the final graphs. Further background information on biological oceanography can be found in the books by Tait (1981), Nybakken (1982) and Thurman (1997), and for additional mathematical details about the theory of dynamical systems consult the books by Guckenheimer and Holmes (1983), Thompson and Stewart (1986), Wiggins (1988, 1990), Glendinning (1994) and Kuznetsov (1995).

2. Model Formulation

The model consists of three coupled ordinary differential equations, describing changes in the concentrations of nutrient (N), phytoplankton (P) and zooplankton (Z) in a physically homogeneous oceanic mixed layer. The interactions between these components are illustrated in Fig. 1. The arrows indicate flows of matter through the system, and the parameterizations of the rates of these flows are indicated on each arrow. The input to the system is the $k(N_0 - N)$ arrow, and arrows not ending in the N, P or Z compartments are losses from the system. The phytoplankton take up nutrient, and are then grazed upon by the zooplankton; the various

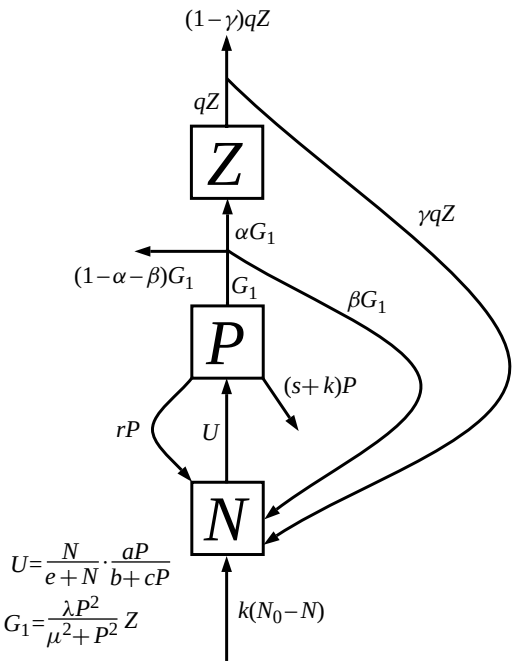

Figure 1. Interactions between nutrients (N), phytoplankton (P) and zooplankton (Z). Arrows indicate flows of matter through the system, and the rates of these flows are labelled. Arrows not starting or not finishing at a compartment indicate input to and losses from the system. U is the phytoplankton uptake function, and G_1 is the zooplankton grazing term.

recycling effects make the situation more complicated than a simple food chain. The flows, equations and subsequent parameter definitions are now discussed, and for brevity we abbreviate Steele and Henderson (1981) to SH81, and Edwards and Brindley (1996) to EB96.

We assume that the mixed layer is thoroughly mixed at all times, so that there are no spatial gradients of concentrations and the changes in N, P and Z can be represented by three coupled ordinary differential equations:

$$\frac{dN}{dt} = -\text{uptake} + \text{respiration} + Z \text{ excretion} + Z \text{ predation excretion} + \text{mixing},$$

$$\frac{dP}{dt} = \text{uptake} - \text{respiration} - \text{grazing by } Z - \text{sinking} - \text{mixing},$$

$$\frac{dZ}{dt} = \text{growth} - \text{higher predation}.$$

The specific functional forms used are:

$$\frac{dN}{dt} = -\frac{N}{e+N}\frac{a}{b+cP}P + rP + \frac{\beta\lambda P^2}{\mu^2+P^2}Z + \gamma qZ + k(N_0 - N), \quad (1)$$

Table 1. Abbreviations, default values and ranges of the parameters. The ranges cover values used by a variety of authors in different models.

Parameter	Symbol	Default value	Reported range
a/b gives maximum P growth rate	a	0.2 m^{-1} day^{-1}	0.07–0.28
Light attenuation by water	b	0.2 m^{-1}	0.04–0.2
P self-shading coefficient	c	0.4 m^2 $(g\ C)^{-1}$	0.3–1.2
Half-saturation constant for N uptake	e	0.03 g C m^{-3}	0.02–0.15
Cross-thermocline exchange rate	k	0.05 day^{-1}	0.0008–0.13
Higher predation on Z	q	0.075 day^{-1}	0.015–0.150
P respiration rate	r	0.15 day^{-1}	0.05–0.15
P sinking loss rate	s	0.04 day^{-1}	0.032–0.08
N concentration below mixed layer	N_0	0.6 g C m^{-3}	0.1–2.0
Z growth efficiency	α	0.25	0.2–0.5
Z excretion fraction	β	0.33	0.33–0.8
Regeneration of Z predation excretion	γ	0.5	0.5–0.9
Maximum Z grazing rate	λ	0.6 day^{-1}	0.6–1.4
Z grazing half-saturation coefficient	μ	0.035 g C m^{-3}	0.02–0.1

$$\frac{dP}{dt} = \frac{N}{e+N}\frac{a}{b+cP}P - rP - \frac{\lambda P^2}{\mu^2+P^2}Z - (s+k)P, \tag{2}$$

$$\frac{dZ}{dt} = \frac{\alpha\lambda P^2}{\mu^2+P^2}Z - qZ. \tag{3}$$

Units of N, P and Z are g C m^{-3}, and time units are days. All parameters are positive, with $\alpha+\beta \leq 1$ and $\gamma \leq 1$ required from their definitions. The original SH81 model considered mesocosm experiments. We have adapted it to the more usual 'open sea' case by incorporating diffusive mixing with deep water, in a similar way to Steele and Henderson (1993). The only difference between our model and that of SH81 is therefore the inclusion of the $-kN$ term in (1) and the $-kP$ term in (2), where k represents the fraction of the mixed layer which is exchanged daily with the deeper water. The equations have not been nondimensionalized, so that when a parameter is varied it is clear exactly which single biological or physical effect is being considered, and avoids the need to translate nondimensional parameters back into dimensional ones.

The parameter definitions are given in Table 1, together with a default value for each parameter, which is that used by SH81. For the numerical investigations we require ranges of values for all of the parameters. To obtain a realistic range EB96 abstracted values from 12 other models, ranging in complexity from a simple two-component model to larger seven-component models. The 12 models considered were those of Steele and Frost (1977), Evans and Parslow (1985), Frost (1987), Hofmann and Ambler (1988), Wroblewski (1989), Fasham *et al.* (1990), Taylor and Joint (1990), Steele and Henderson (1992, 1993), Fasham (1993), Armstrong (1994), and Henderson and Steele (1995).

The broad ranges of values shown in Table 1 partly reflect different geographical or other physical influences, but are somewhat due to the uncertainties of parameter estimation. Since N, P and Z are measured in units of g C m^{-3}, the parameters are converted into the appropriate units using the conversion equivalences of SH81, namely 1 g carbon $\equiv$ 20 mg chlorophyll $\equiv$ 10 mmol nitrogen.

Following SH81 and EB96 we consider a fixed mixed-layer depth of 12.5 m, corresponding to summer conditions. The mixed layer deepens considerably during the winter, and inclusion of this process explicitly into the model would require a forcing (time-dependent) function, plus incorporation of a dilution rate of the N, P and Z concentrations, as proposed by Evans and Parslow (1985). However, it is helpful to first understand the behaviour of the unforced system, and we defer consideration of a varying mixed-layer depth to a later paper [in preparation, based on Edwards (1997)], where the understanding of the dynamics of the unforced system provides insights into the behaviour of the forced system. The mixed-layer depth is implicitly incorporated in the values of a, k and s, as discussed shortly. The precise parameter values obtained from the papers cited above were given in detail in EB96 and Edwards (1997) to produce the parameter ranges, and are not repeated here. Two minor modifications to the ranges of a and α used by EB96 are explained. We now briefly describe the terms in equations (1), (2) and (3), in the order in which they appear in the equations.

A Michaelis–Menten function $N/(e+N)$ models nutrient uptake by phytoplankton, where e is the half-saturation constant. The term $a/(b+cP)$ represents (non-nutrient limited) phytoplankton growth with limitations due to light attenuation by the water, b, and self-shading of the phytoplankton, c. The value of a/b gives the maximum daily growth rate averaged over the depth of the mixed layer. Light attenuation by the water is represented by b, where $b = (\ln 100)/z_e$ corresponds to the 1% light maximum at a depth of z_e metres (taken by SH81 to be 20 m, giving $b = 0.2$ m^{-1}). The term cP represents phytoplankton self-shading; as the phytoplankton concentration increases, the average light received per organism, and therefore the average growth rate, is reduced.

The term $a/(b+cP)$ was equated by SH81 to the depth-averaged daily phytoplankton growth rate $2.58V_p/(b+cP)Z_m$ derived by Steele and Frost (1977), where V_p is the maximum phytoplankton growth rate under optimal light conditions and Z_m represents the depth of the mixed layer. However, this derivation was implicitly based on the equation for the photosynthesis-light curve given by Steele (1962) which, as Platt and Sathyendranath (1993) have indicated, should be avoided because it includes photoinhibition and has no extended range of light-saturation. Also, the equation of Steele (1962) implies that the maximum photosynthesis rate occurs at a depth which is independent of the surface irradiance, which should not be the case. However, Edwards (1997) has shown that the functional form $a/(b+cP)$ can still be used, as it can be obtained from the canonical form for primary production derived by Platt *et al.* (1990) and Platt and Sathyendranath (1993). This provides a formulation of our parameter a in a way that allows its value to

be explicitly calculated for any location and for any time of the year. In EB96 we inadvertently equated some values of V_p used by other authors to a/b when constructing a range of values for a. Values which do equate to a/b were used by Steele and Henderson (1992), Armstrong (1994) and Henderson and Steele (1995); these values were, respectively, 0.35 day^{-1}, 1.4 (and 0.7 for a micronutrient-limited case) and 0.5. Keeping b fixed at its default value, these yield a range of values for a of 0.07–0.28, narrower than the range used in EB96 (which was 0.1–0.6).

The default respiration rate, r, is 0.15 day^{-1}. Fasham *et al.* (1990) had no respiration term as such, but they did have an equivalent natural mortality rate of 0.09 day^{-1}, some of which was subsequently recycled back through the microbial loop. Our respiration term is recycled immediately into nutrient [as were those of Evans and Parslow (1985) and Henderson and Steele (1995)], whilst none of our linear sinking term, s, is recycled. We consider r to represent both respiration and natural mortality, because both processes are modelled by other authors as linear losses.

A sigmoidal Holling type III zooplankton grazing term, $\lambda P^2/(\mu^2 + P^2)$, is used, with maximum zooplankton grazing rate λ, and half-saturation constant μ. The type III form is chosen by SH81 [and Steele and Henderson (1993)] based on the zooplankton grazing data presented by Adams and Steele (1966), which indicates low grazing rates at low phytoplankton concentrations.

The fraction α of zooplankton grazing represents the growth efficiency of the zooplankton, and the fraction β of zooplankton grazing represents zooplankton excretion, which is regenerated immediately into the nutrient compartment. The remaining fraction $1-\alpha-\beta$ models zooplankton faecal pellets, which are assumed to sink out of the mixed layer. Fasham (1993) used a zooplankton *assimilation* efficiency of 0.75 to multiply the zooplankton grazing term, assuming also that zooplankton excretion was a constant proportion of zooplankton biomass (rather than a proportion of consumption, such as our β). In EB96 we included the Fasham (1993) value of 0.75 when constructing our range for α, but, being an assimilation efficiency rather than a growth efficiency, it should not have been. We thus now consider a range for α of 0.2–0.5, based upon the values used by Evans and Parslow (1985) and Steele and Henderson (1992, 1993), which is consequently smaller than the range used in EB96.

Zooplankton mortality due to predation by higher predators is modelled by the linear function qZ, where q is the mortality rate and has units of day^{-1}. This function replaces the quadratic function dZ^2 used in EB96, where d is the mortality rate and has units of (g C m^{-3})$^{-1}$ day^{-1}. The two alternative functions represent different assumptions about zooplankton mortality. The quadratic form dZ^2 assumes that the carnivorous predator population changes in size in proportion to the zooplankton population, whereas the linear form qZ assumes a constant rate of predation. SH81 showed, for their mesocosm case, that numerical simulations of the system significantly changed behaviour at different values of d. Their results, together with the fact that d is a particularly difficult parameter to measure and assign a fixed value

to [Steele and Henderson (1993) stated that in any model it is essentially a free choice], motivated us to use d as the primary bifurcation parameter in EB96, and so here we shall equivalently use q as our primary bifurcation parameter. Steele and Henderson (1981, 1992) discussed the use of either the linear or the quadratic function. Returning to the earlier list of models, we find the following values of the daily zooplankton loss rate, q, to have been used when the linear zooplankton mortality term was considered: 0.04 day^{-1} by Wroblewski (1989), 0.05 by Fasham *et al.* (1990) and 0.07 by Evans and Parslow (1985). However, subtle differences in the equations used mean that these values cannot be simply taken at face value, as is now discussed.

Fasham *et al.* (1990) also included a linear zooplankton excretion rate of 0.1 day^{-1}, making a total loss rate of 0.15. However, our zooplankton excretion is an assumed proportion, β, of zooplankton grazing rather than a proportion of zooplankton biomass. Fasham (1993) retained the Fasham *et al.* (1990) assimilation efficiency of 0.75, but the zooplankton loss term (including excretion and losses due to higher predators) was changed from a linear form to a Michaelis–Menten (or Holling type II) function, with a maximum loss rate of 0.3 day^{-1}. This maximum was only attained in the simulations during summer at Ocean Weather Station "India"; for the Bermuda simulations, the loss rate peaked above 0.15 day^{-1} [the constant total loss rate of Fasham *et al.* (1990)] only during April and May. Wroblewski (1989) had an 'unassimilated fraction' of zooplankton grazing of 0.3 recycled to nutrient, with the remaining 0.7 fuelling zooplankton growth, but no zooplankton excretion. Evans and Parslow (1985) had a 'grazing efficiency' of 0.5, twice as high as our growth efficiency, and no specific excretion term.

With the quadratic mortality function dZ^2, Fig. 3(c) of EB96 shows a fairly constant steady-state value of Z of roughly 0.075 g C m^{-3} as d varies across its range of 0.25–2.0 (with all other parameters set to their default values). The parameter d had the default value 1.0. The substitution of the linear form for the quadratic form is a qualitative difference, and it is desirable to minimize quantitative differences when comparing the two cases of linear and quadratic mortality. This is achieved by taking a default value of $q = 0.075$, so that we have $qZ \simeq dZ^2$, and a range for q of 0.015–0.150. This is a reasonable range to consider given the aforementioned values used by other authors and the practical difficulties in obtaining measurements for q. The parameter γ, which multiplies qZ in (1), is the proportion of the zooplankton mortality that is regenerated as nutrient via excretion of the higher predators. The remaining fraction $1 - \gamma$ fuels the growth of the higher predators.

The $k(N_0 - N)$ term models the exchange of nutrients with the water below the mixed layer, where the exchange rate k defines the fraction of the mixed layer which is exchanged daily with the deeper water due to diffusive processes, and N_0 is the sub-mixed-layer nutrient concentration. Our range of k given in Table 1 implicitly incorporates the fixed mixed-layer depth of 12.5 m, as does the range for s, the sinking rate of phytoplankton out of the mixed layer. SH81 took $s = 0.04$ day^{-1},

corresponding to a sinking velocity of 0.5 m day^{-1} (because a fraction 0.04 of the phytoplankton drop out of the bottom of the mixed layer each day).

3. Analysis—Existence and Stability of Steady States

A thorough algebraic investigation into the nature of the steady states, without using any numerical parameter values, is given by Edwards (1997); here we summarize the results without giving the detailed proofs. The analysis is based on that of a general class of models by Truscott and Brindley (1994), and parallels that of the quadratic mortality case in EB96. The incorporation of the self-shading term $a/(b + cP)$ in our model means that the analysis of Truscott and Brindley (1994) cannot be used directly, but requires minor adaptations. For readers with a stronger biological than mathematical background, this section may be skimmed without greatly diminishing understanding of the numerical results of Sections 4–7.

Steady states are solutions (N, P, Z) to $dN/dt = dP/dt = dZ/dt = 0$. The local stability of a steady state is determined by the eigenvalues of the Jacobian matrix, which is given by

$$\mathbf{A} = \begin{bmatrix} -\frac{aeP}{(e+N)^2(b+cP)} - k & -\frac{abN}{(e+N)(b+cP)^2} + r + \frac{2\beta\lambda\mu^2 PZ}{\left(\mu^2+P^2\right)^2} & \frac{\beta\lambda P^2}{\mu^2+P^2} + \gamma q \\ \frac{aeP}{(e+N)^2(b+cP)} & \frac{abN}{(e+N)(b+cP)^2} - r - s - k - \frac{2\lambda\mu^2 PZ}{\left(\mu^2+P^2\right)^2} & -\frac{\lambda P^2}{\mu^2+P^2} \\ 0 & \frac{2\alpha\lambda\mu^2 PZ}{\left(\mu^2+P^2\right)^2} & \frac{\alpha\lambda P^2}{\mu^2+P^2} - q \end{bmatrix},$$

evaluated at the steady state values of N, P and Z. Steady states with $Z = 0$ will have the same definitions as those for the quadratic case in EB96, because the only difference between the linear and quadratic models is the qZ and dZ^2 terms, which are both zero when $Z = 0$. However, the third column of $\mathbf{A}$ is different from that for the quadratic case, and so the stability of steady states with $Z = 0$ can be different.

The steady state $(N, P, Z) = (N_0, 0, 0)$ exists for all parameter values, and the Jacobian at $(N_0, 0, 0)$ is

$$\mathbf{A} = \begin{bmatrix} -k & -\frac{aN_0}{b(e+N_0)} + r & \gamma q \\ 0 & \frac{aN_0}{b(e+N_0)} - r - s - k & 0 \\ 0 & 0 & -q \end{bmatrix}.$$

As this matrix is upper triangular, the eigenvalues are $-k$, Φ and $-q$, where

$$\Phi = \frac{aN_0}{b(e + N_0)} - r - s - k.$$

Thus, the stability depends on the sign of Φ; for $\Phi < 0$ $(N_0, 0, 0)$ is a stable node and for $\Phi > 0$ it is a saddle point, and therefore unstable. Φ is positive for the

default parameter values, and remains positive as any one parameter is varied over its range; this is the same behaviour as for the quadratic case in EB96. For $\Phi < 0$, $(N_0, 0, 0)$ is the only steady state in the positive octant, and it is stable.

Setting $Z = 0$ and eliminating P from $dN/dt = 0$ and $dP/dt = 0$, results in the following quadratic equation:

$$ckN^2 + \left[\frac{a(s+k)}{r+s+k} - b(s+k) + ck(e - N_0)\right]N - (b(s+k) + ckN_0)e = 0, \tag{4}$$

the solutions of which we denote by $N_1{}^*$ and $N_2{}^*$. These solutions correspond to the two steady states $(N_1{}^*, P_1{}^*, 0)$ and $(N_2{}^*, P_2{}^*, 0)$, where $P_1{}^*$ and $P_2{}^*$ are given by

$$P_i{}^* = \frac{k(N_0 - N_i{}^*)}{s+k} \tag{5}$$

for $i = 1, 2$. The constant term of (4) is negative, and so it has two real roots, one negative and one positive. Defining $N_1{}^*$ to be the positive root of (4) and $N_2{}^*$ to be the negative root, then the steady state $(N_2{}^*, P_2{}^*, 0)$ can never enter the positive octant $\{N, P, Z \geq 0\}$ of phase space, and as such remains ecologically unrealistic and is considered no further. Further calculations show that the sign of $P_1{}^*$ is given by the sign of Φ, and that as $\Phi \to 0$ we have $P_1{}^* \to 0$, and $N_1{}^* \to N_0$, i.e., $(N_1{}^*, P_1{}^*, 0) \to (N_0, 0, 0)$.

The stability of $(N_1{}^*, P_1{}^*, 0)$ is determined solely (for $P_1{}^* > 0$) by the sign of the (3, 3) component of **A**, because the other two eigenvalues always have negative real parts (Edwards, 1997). As such, $(N_1{}^*, P_1{}^*, 0)$ is stable for $P_1{}^* > 0$ if and only if

$$\frac{\alpha\,\lambda\,P_1{}^{*2}}{\mu^2 + P_1{}^{*2}} - q < 0. \tag{6}$$

So at small enough values of $P_1{}^*$, $(N_1{}^*, P_1{}^*, 0)$ is stable. As $\Phi \to 0^+$, $(N_1{}^*, P_1{}^*, 0) \to (N_0, 0^+, 0)$, and for $\Phi < 0$ we have $P_1{}^* < 0$ and the steady state $(N_1{}^*, P_1{}^*, 0)$ is outside the positive octant. $(N_0, 0, 0)$ is unstable for $\Phi > 0$ and stable for $\Phi < 0$. Thus, at $\Phi = 0$ we have a transcritical bifurcation, whereby $(N_1{}^*, P_1{}^*, 0)$ exchanges stability with $(N_0, 0, 0)$. The local picture around this bifurcation can be summarized as

- $\Phi < 0$ – $(N_0, 0, 0)$ stable, $(N_1{}^*, P_1{}^*, 0)$ ecologically unrealistic $(P_1{}^* < 0)$;
- $\Phi > 0$ – $(N_0, 0, 0)$ unstable, $(N_1{}^*, P_1{}^*, 0)$ realistic and stable.

In the numerical investigation we use the higher predation on zooplankton parameter q as the primary bifurcation parameter. Setting all parameters except q to their default values, solving (4) and (5) gives the steady state

$$(N_1{}^*, P_1{}^*, 0) = (0.0196, 0.322, 0), \tag{7}$$

which is independent of q. However, the stability does depend on q, and we can state from (6) that $({N_1}^*, {P_1}^*, 0)$ is stable if and only if $q > 0.148$.

For steady-state solutions of the form (N^*, P^*, Z^*) with $Z^* \neq 0$, $dZ/dt = 0$ gives

$$P^* = \sqrt{\frac{q}{\alpha\lambda - q}}\,\mu, \tag{8}$$

where the positive root is taken. (The steady state obtained from the negative root will have a negative P value for all parameter values, and so can never enter the positive octant). P^* clearly exists if and only if $q < \alpha\lambda$. Edwards (1997) showed how the corresponding N^* and Z^* values are determined from solving $dN/dt = 0$ and $dP/dt = 0$, that $N^* > 0$ always holds, and that $Z^* > 0$ if and only if $\Omega > 0$, where

$$\Omega = \left(N_0 - \frac{(s+k)}{k}P^*\right)\left[\frac{a}{b + cP^*} - (r+s+k)\right] - (r+s+k)e. \tag{9}$$

Furthermore, the positive values of N^* and Z^* are always unique, and hence there is at most one steady state (N^*, P^*, Z^*) with $N^*, P^*, Z^* > 0$; this contrasts with the quadratic mortality case in EB96, for which multiple steady states were numerically shown to occur in the strictly positive octant $\{N, P, Z > 0\}$ for some parameter values. Thus, for the linear case we know that if we numerically find a steady state with $N^*, P^*, Z^* > 0$, then that is the unique steady state in the strictly positive octant, and will not undergo fold (saddle-node) bifurcations in the octant.

The steady states $({N_1}^*, {P_1}^*, 0)$ and (N^*, P^*, Z^*) pass through each other at a transcritical bifurcation, which occurs when parameters are such that $\Omega = 0$. The local behaviour around this transcritical bifurcation is summarized as

- $\Omega < 0 -$ $({N_1}^*, {P_1}^*, 0)$ stable, (N^*, P^*, Z^*) ecologically unrealistic $(Z^* < 0)$;
- $\Omega > 0 -$ $({N_1}^*, {P_1}^*, 0)$ unstable, (N^*, P^*, Z^*) realistic and stable.

So, the conditions for the existence of $(N_0, 0, 0)$, $({N_1}^*, {P_1}^*, 0)$ and $({N_2}^*, {P_2}^*, 0)$ are the same as for the quadratic zooplankton mortality case of EB96, as expected because $Z = 0$. The stability of $(N_0, 0, 0)$ is the same for both models. However, for the quadratic case $({N_1}^*, {P_1}^*, 0)$ could never become stable, whereas for the current linear case it can be stable. The two transcritical bifurcations at $\Phi = 0$ and $\Omega = 0$ are graphically depicted in bifurcation diagrams in Edwards (1997), showing how the steady state (N^*, P^*, Z^*) leaves the positive octant as Ω decreases through zero. For the quadratic mortality case, the two separate transcritical bifurcations do not occur, but a 'three-way transcritical bifurcation' occurs at $\Phi = 0$, at which point all three steady states $(N_0, 0, 0)$, $({N_1}^*, {P_1}^*, 0)$ and (N^*, P^*, Z^*) exchange stability.

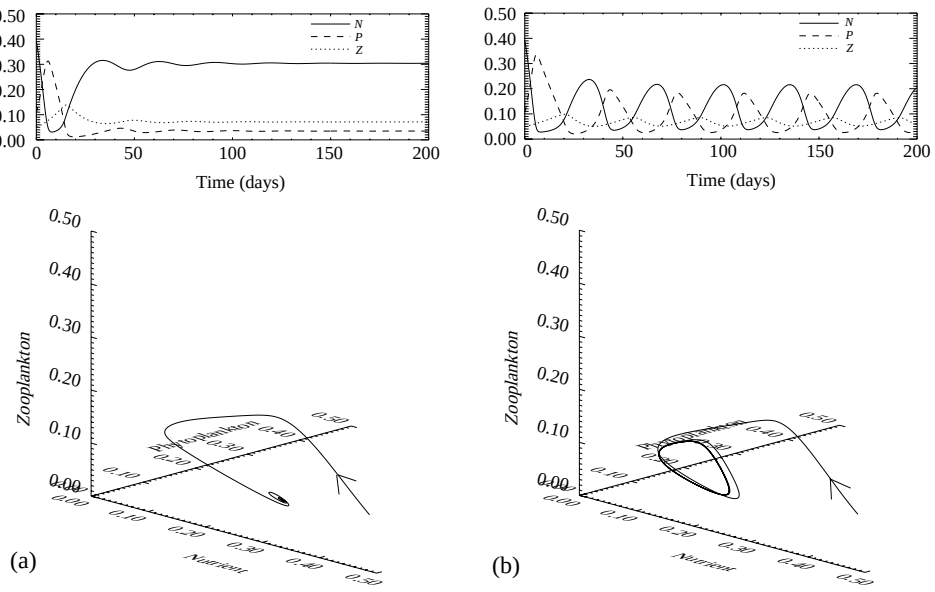

Figure 2. The time series and phase-space trajectory at two values of q, with all of the other parameters fixed at their default values. (a) $q = 0.075$—N, P and Z settle down to steady-state values. (b) $q = 0.11$—the system settles down to a stable limit cycle.

4. TIME SERIES AND PHASE PORTRAITS

In Fig. 2(a) we plot the time series and the trajectory in $N - P - Z$ space of the system from the initial condition $(N, P, Z) = (0.4, 0.1, 0.05)$, with all of the parameters fixed at their default values—in particular $q = 0.075$. Here, and in all diagrams, units of N, P and Z are g C m^{-3}. After a transient time N, P and Z settle down to steady-state values of $(N, P, Z) = (0.30, 0.035, 0.071)$.

These are almost exactly the default steady state values obtained in the quadratic case of EB96, but this is not surprising given that the default value of q is such that $qZ \simeq dZ^2$, where dZ^2 is the quadratic zooplankton mortality term. However, the transient time is longer than that for the quadratic case, which is due to differences in the eigenvalues at the steady states. The initial large increase in P is due to the excitable nature of the system; starting from the alternative initial condition $(N, P, Z) = (0.4, 0.1, 0.1)$, i.e., at a higher value of Z, this increase in P does not occur, and the steady state is reached much more quickly [see Truscott and Brindley (1994) and Edwards (1997)].

From the preceding analysis, we know that there are two other steady states with non-negative values of N, P and Z, namely $(N_0, 0, 0)$ and $({N_1}^*, {P_1}^*, 0)$, but that these are both unstable at the default parameter values. We also know that $(N^*, P^*, Z^*) = (0.30, 0.035, 0.071)$ is the unique steady state in the strictly positive octant $\{N, P, Z > 0\}$. The analysis further shows that if q is then decreased from its default value of 0.075, then (N^*, P^*, Z^*) will stay in the strictly posi-

tive octant and remain stable (although the actual values of N^*, P^* and Z^* will change).

In Figure 2(b) the value of q is increased to 0.11, and the system integrated from the same initial conditions. The value $q = 0.11$ was chosen because it is roughly one and a half times the default value of 0.075, and for the quadratic case EB96 showed the equivalent trajectories for $d = 1.0$ and $d = 1.5$. As for the quadratic case, at the higher level of predation on zooplankton the variables exhibit oscillatory behaviour. The trajectory is attracted onto a limit cycle, with a period of roughly 35 days.

The trajectory exhibits large-amplitude fluctuations in N, at values lower than the default steady-state value in Fig. 2(a), and small oscillations in Z about the default steady-state value. The oscillations in P have a much larger amplitude than those for $d = 1.5$ in the quadratic case. EB96 showed that for any value of d (with the other parameters kept at their default values), the maximum value of P attained during a limit cycle was 0.125, significantly less than the 0.18 value attained in Fig. 2(b) for linear zooplankton mortality. We shall pursue this point further in the following section.

5. One-parameter Bifurcation Behaviour

There is a qualitative difference between Figs 2(a) and 2(b); the change from a steady state to oscillatory behaviour suggests that there has been a Hopf bifurcation at some value of q between 0.075 and 0.11. A Hopf bifurcation occurs when, as a parameter is increased or decreased, a steady state changes its stability yielding a branch of periodic orbits close to the bifurcation. We now construct bifurcation diagrams in which q is varied continuously, indicating the value of q at which a Hopf bifurcation does indeed occur, and showing the steady-state values and limit cycle ranges of N, P and Z as q is varied.

Figure 3(a) shows how the steady-state value of the nutrient concentration, defined as N^*, varies as q changes, with all of the other parameters kept fixed at their default values. At $q = 0.075$, $N^* = 0.30$, as indicated by Fig. 2(a). The solid line passing through $q = 0.075$ in Fig. 3(a) indicates that the steady state is stable. As q increases from 0.075, the steady state goes from being stable (solid line) to unstable (dashed line) via a Hopf bifurcation (solid square) at $q = 0.0841$, labelled A, and then regains stability at a second Hopf bifurcation at $q = 0.130$, labelled B. At $q = 0.11$ Fig. 2(b) showed that trajectories are attracted onto a stable limit cycle. This is indicated in Fig. 3(a) by the solid circles, which represent the maximum and minimum nutrient concentrations attained along the limit cycle. The branch of stable limit cycles arising from Hopf bifurcation A persists as q is increased, and then collapses onto Hopf bifurcation B. No secondary bifurcations of the limit cycles, such as period-doubling bifurcations, occur.

The steady-state curve in Fig. 2(a) ends at $q = 0.148$ since at this point Z^* passes through zero and (N^*, P^*, Z^*) is no longer ecologically realistic, because

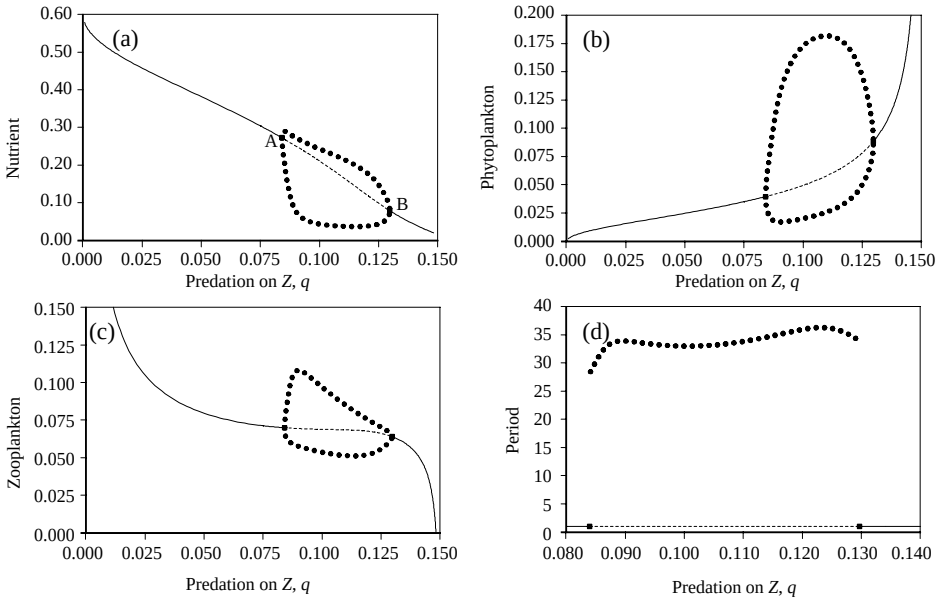

Figure 3. Variations in the steady-state values of (a) nutrient, (b) phytoplankton and (c) zooplankton as q, the higher predation on the zooplankton, is changed. A solid line is a stable steady state, a dashed line is an unstable steady state, a solid square is a Hopf bifurcation and solid circles indicate the maximum and minimum values of the stable limit cycles. The Hopf bifurcations are labelled A and B. (d) The period of the limit cycles (solid circles) remains virtually constant throughout the region of oscillatory behaviour; the corresponding stability of the steady state is indicated by the horizontal line.

Ω, as defined by (9), goes through zero. This point is the transcritical bifurcation calculated in Section 3, and stability is transferred to $({N_1}^*, {P_1}^*, 0)$, which remains stable for $q > 0.148$.

Figures 3(b) and 3(c) are the equivalent diagrams for phytoplankton and zooplankton, which have default steady-state values of $P^* = 0.035$ and $Z^* = 0.071$. The maximum values of P and Z attained along the limit cycles are much higher than the (unstable) steady-state values between the two Hopf bifurcations.

Figure 3(d) shows how the period of the limit cycles changes as q varies between the values at which the Hopf bifurcations occur (the only relevant range of q). It is seen that the period is fairly insensitive to the value of q. The sensitivity of the period to each of the other parameters shall be shown by period–contour diagrams in Section 7.

The bifurcational behaviour is very similar to that for the quadratic case in EB96, for which the Hopf bifurcations and consequent limit cycles also occur. The general features of the bifurcation diagrams are the same, with the oscillations occurring across a wider range of q than the corresponding relative range of d for the quadratic case. We say 'relative range' because q and d have different units.

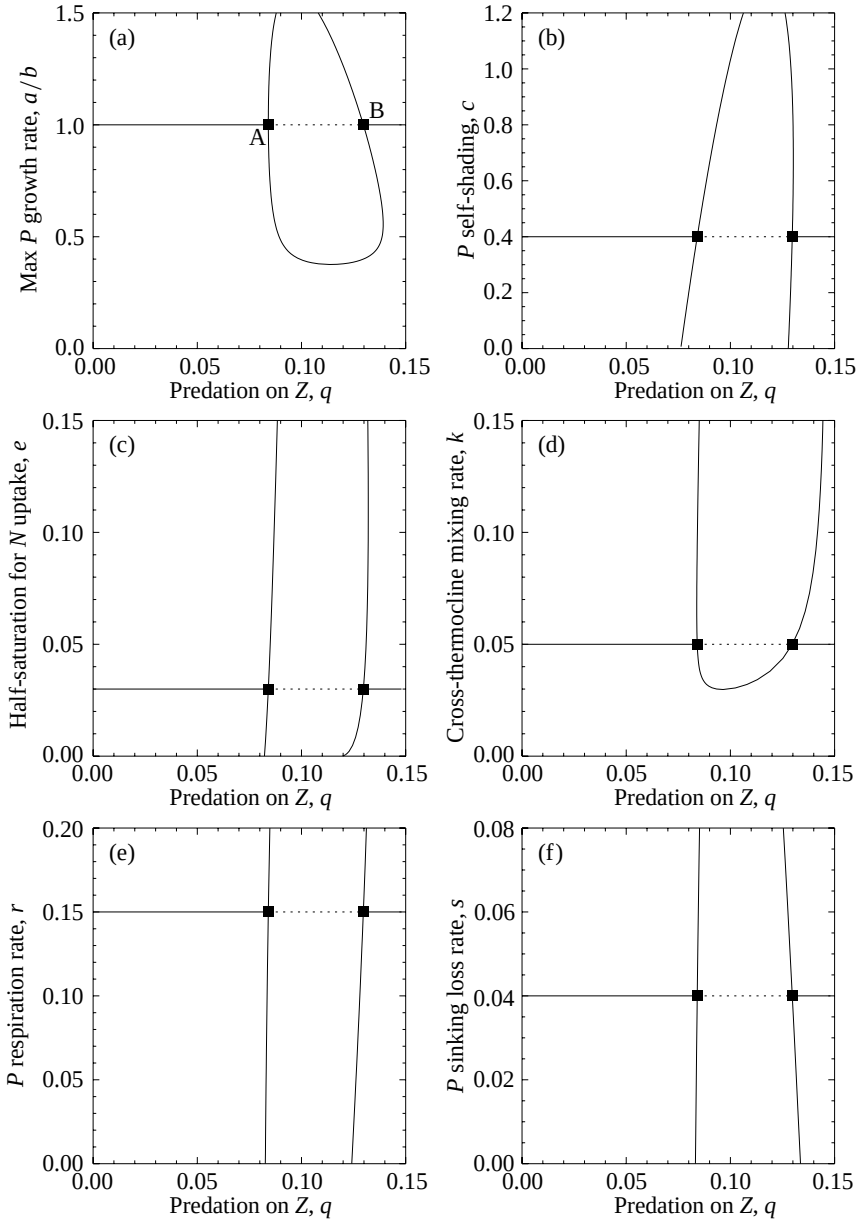

Figure 4. Two-parameter bifurcation diagrams showing how the positions of the Hopf bifurcations in Fig. 3 change as each other parameter, together with q, is independently varied from its default value. The steady-state stabilities from Fig. 3 are shown as a horizontal line at each default parameter value. Hopf A and Hopf B are indicated in (a). Non-horizontal solid curves starting from the original Hopf bifurcations (the squares) indicate supercritical Hopf bifurcations, and the non-horizontal curve of short dashes in (l) shows where a Hopf bifurcation is subcritical. No fold bifurcations of the steady state occur.

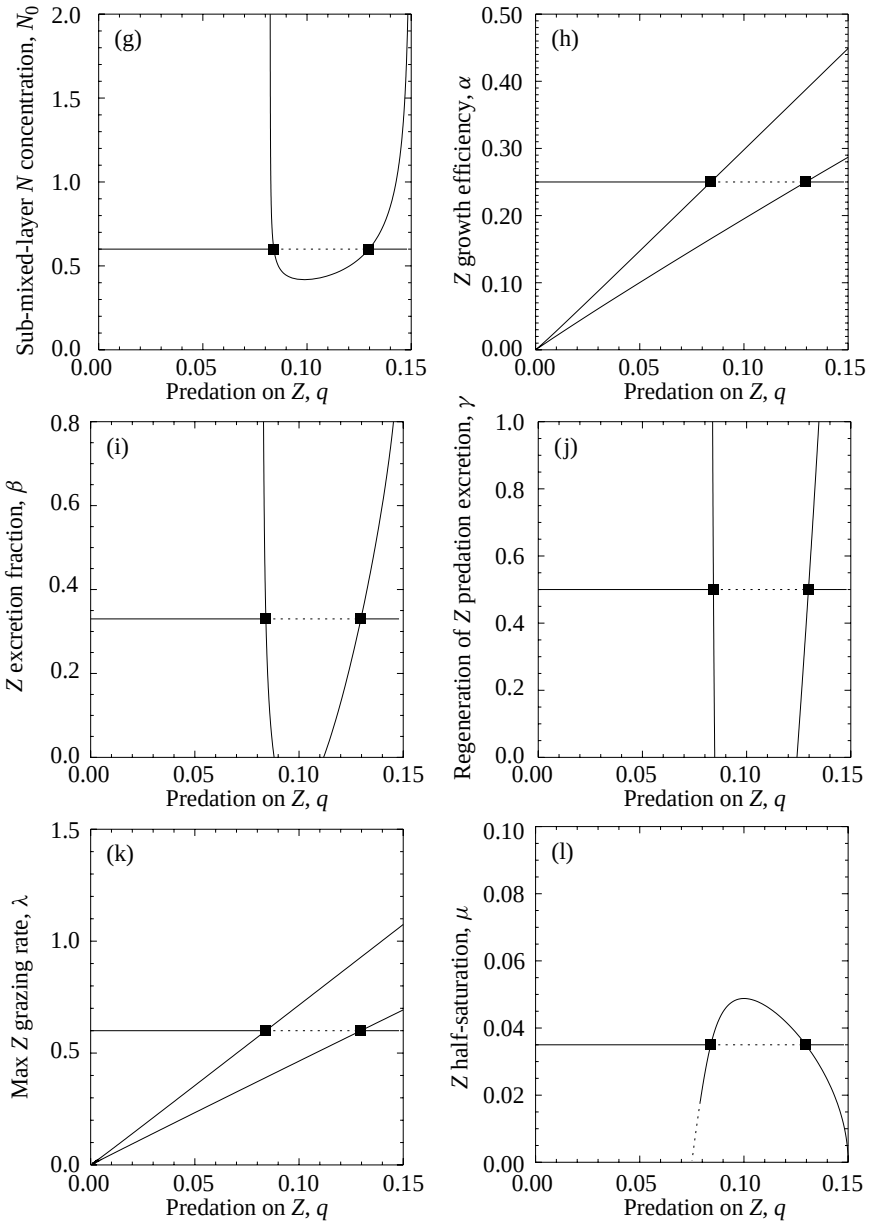

Figure 4. Continued

The amplitudes of the cycles are greater for the linear case than the quadratic case, with all three variables reaching higher maximum values and lower minimum values. The amplitude of fluctuations in Z for the quadratic case were relatively small, but for the linear case they are much more pronounced. Apart from at high q values, the Z^* steady-state pictures for the two cases are similar. Since the default

value and range of q are taken such that $qZ \simeq dZ^2$, this similarity may not seem too surprising, but on the other hand there is a qualitative difference in the way in which Z^* is calculated from the equations, and so such similarity between the linear and quadratic cases may be slightly unexpected. For the quadratic case, Z^* does not reach zero as d is increased, because the transcritical bifurcation present at $\Omega = 0$ for the linear case does not occur.

6. TWO-PARAMETER BIFURCATION BEHAVIOUR

In Fig. 4 we show how the locations of the two Hopf bifurcations change as each of the parameters, together with q, is independently varied across the ranges reported in Table 1. The axis range plotted for each parameter is from zero to (approximately) its maximum reported value. Figure 4 thus indicates how the qualitative nature of the steady-state bifurcation diagrams depicted in Fig. 3 will change as one other parameter is varied.

For each parameter, the bifurcation diagram from Fig. 3 is shown as a horizontal line at the default value of the parameter, because the parameter was held constant in Fig. 3. A solid horizontal line represents a stable equilibrium, a dashed horizontal line is an unstable equilibrium, and squares again represent the Hopf bifurcations, labelled A and B in Fig. 4(a). In the region of q where the equilibrium is unstable, limit cycles occur, as illustrated in Fig. 3.

In Fig. 3(c) we see that Z^* passes through zero at $q = 0.148$. We know from the analysis that this is a transcritical bifurcation, whereby stability is transferred from (N^*, P^*, Z^*) to $({N_1}^*, {P_1}^*, 0)$ as (N^*, P^*, Z^*) leaves the positive octant. This bifurcation occurs at $\Omega = 0$, which gives $q = 0.148$ when all other parameters are set to their default values. The horizontal line in each diagram of Fig. 4, representing the stability of (N^*, P^*, Z^*) at the default parameter values, therefore terminates at $q = 0.148$. This can be most clearly seen in Fig. 4(i) for β, and is less clear in the other diagrams due to the location of tick marks on the right-hand axes. We know that $({N_1}^*, {P_1}^*, 0)$ is then locally stable for $q > 0.148$. The value of q for which $\Omega = 0$, will change when any of the parameters that appear in the definition of Ω are varied, as illustrated by further diagrams in Edwards (1997).

In each diagram of Fig. 4 the positions of the two Hopf bifurcations are tracked as both q and one other parameter are varied. A nonhorizontal solid line shows the location of a (supercritical) Hopf bifurcation. All Hopf bifurcations are supercritical (as in Fig. 3), except in Fig. 4(l) for μ, where the dashed line indicates that Hopf A becomes subcritical (to be explained shortly). The effects of variations in a and b have been combined as a/b in a single diagram for the maximum phytoplankton growth rate, so that there are 12 distinct bifurcation diagrams.

Firstly consider Fig. 4(b), the diagram for c, the phytoplankton self-shading parameter, against q. Figure 4(b) shows that the two Hopf bifurcations occur for all values of c. The q-value of Hopf B remains fairly constant across all values of

c, whereas the q-value of Hopf A increases as c increases. Therefore, the range of q for which the steady state is unstable and oscillations occur (i.e., the interval between the two Hopf bifurcations) becomes narrower as c increases. We say that 'oscillations occur' across a region, although the branches of limit cycles which emanate from the Hopf bifurcations may themselves undergo further bifurcations; we examine such bifurcations of limit cycles in Section 7, and for now refer to the area between the curves of Hopf bifurcations as a region of oscillations.

Oscillations occur across the full ranges of five of the other parameters, namely e, r, s, β and γ, as indicated by Figs 4(c), (e), (f), (i) and (j) respectively. Figure 4(a) shows that at low values of a/b the Hopf bifurcations do not occur. As a/b is decreased from its default value, the region of oscillations widens slightly, and then the two Hopf bifurcations come together. Similar behaviour also occurs for k and N_0, Figs 4(d) and (g). Figures 4(h) and (k), for α and λ, are similar, in that a reduction of either parameter causes both Hopf bifurcations to shift to the left, resulting in a narrowing of the oscillatory region.

Finally, Fig. 4(l) shows that an increase in μ causes the Hopf bifurcations to come together, and so (N^*, P^*, Z^*) is stable for large values of μ. As μ decreases, the curve of short dashes indicates that Hopf A becomes subcritical. This means that if μ is fixed at a low value and the one-parameter bifurcation diagram of N against q computed [i.e., the equivalent diagram to Fig. 3(a)], this diagram would be qualitatively different to that of Fig. 3(a). In Fig. 3(a) Hopf A is supercritical, which means that a branch of stable limit cycles (the solid circles) emanates from it. For a subcritical Hopf bifurcation, the cycles would be unstable, and would head to the left of Hopf A, coexisting with the stable steady state. This situation can then result in a stable limit cycle and a stable steady state both occurring at the same parameter values, and trajectories will be attracted to one or the other depending on the initial conditions. However, the minimum value of μ given in Table 1 is 0.02, and so the values of μ for which Hopf A is subcritical are actually below the realistic range of μ. Therefore, both Hopf bifurcations remain supercritical across the realistic ranges of all the diagrams in Fig. 4.

Figure 4 gives us a broad picture of the dynamical behaviour of the model across ranges of all of the parameters. The Hopf curves are, on the whole, fairly 'vertical', and so the Hopf bifurcations will, when they occur, tend to be close to the same values of q as for the default values, i.e., the values of $q = 0.084$ and $q = 0.130$ shown in Fig. 3. We now compare this broad picture with the equivalent one for the quadratic zooplankton mortality model, shown in Fig. 5. This is essentially Fig. 4 in EB96, but with the corrected ranges for a/b and α discussed in Section 2.

The most striking difference between Figs 4 and 5 is that the steady state is unstable, and hence oscillations occur, across a larger range of parameters for the linear case than for the quadratic case. Oscillations occur across the full ranges of six of the parameters in the linear case, but only for r, s and γ in the quadratic case. However, there are broad similarities between the linear and quadratic diagrams,

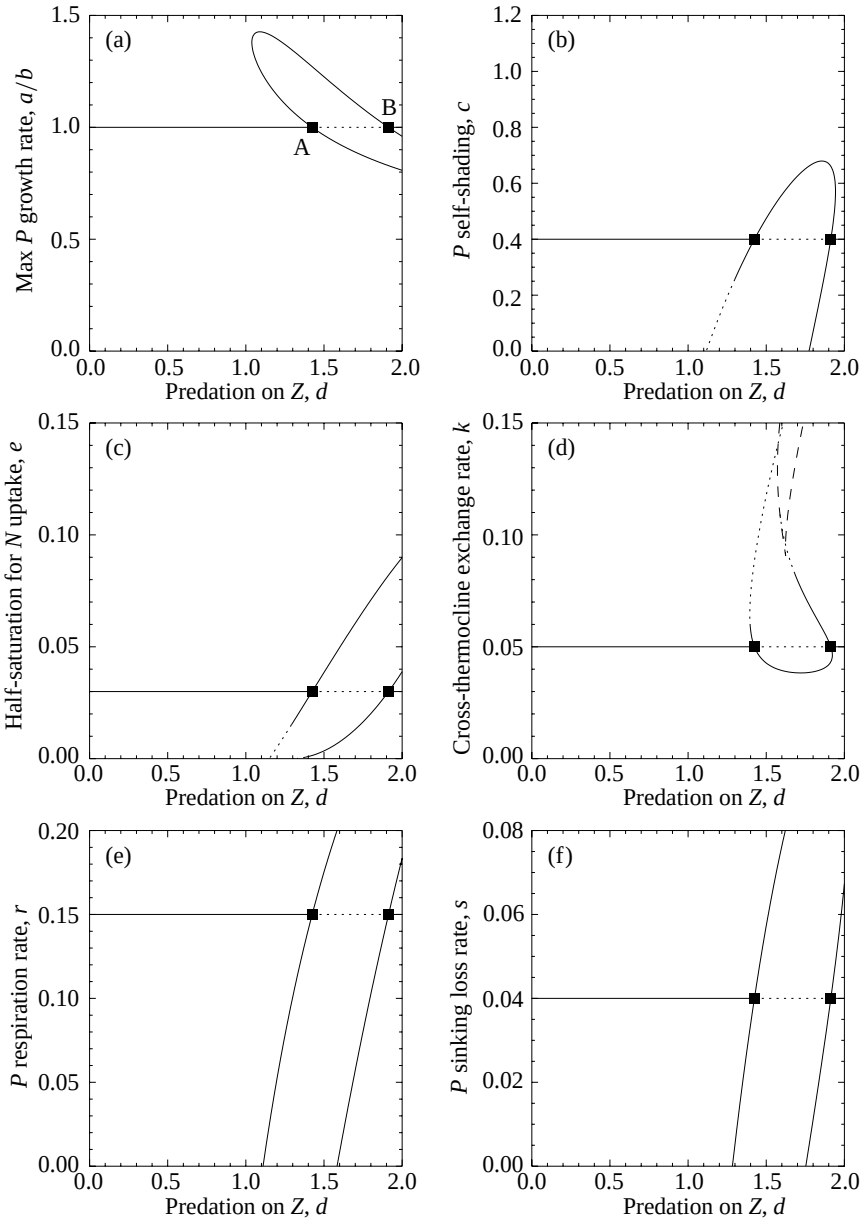

Figure 5. The equivalent two-parameter bifurcation diagrams for the quadratic zooplankton mortality model. The key and the axes scales are the same as for Fig. 4, and curves of long dashes indicate fold bifurcations of the steady state.

in that the linear diagrams are, in some sense, stretched versions of the quadratic ones.

Subcritical Hopf bifurcations are common in the quadratic case, occurring for six of the parameters, but do not appear within the realistic ranges for the linear case. And unlike the linear case, the quadratic case exhibits fold bifurcations of the

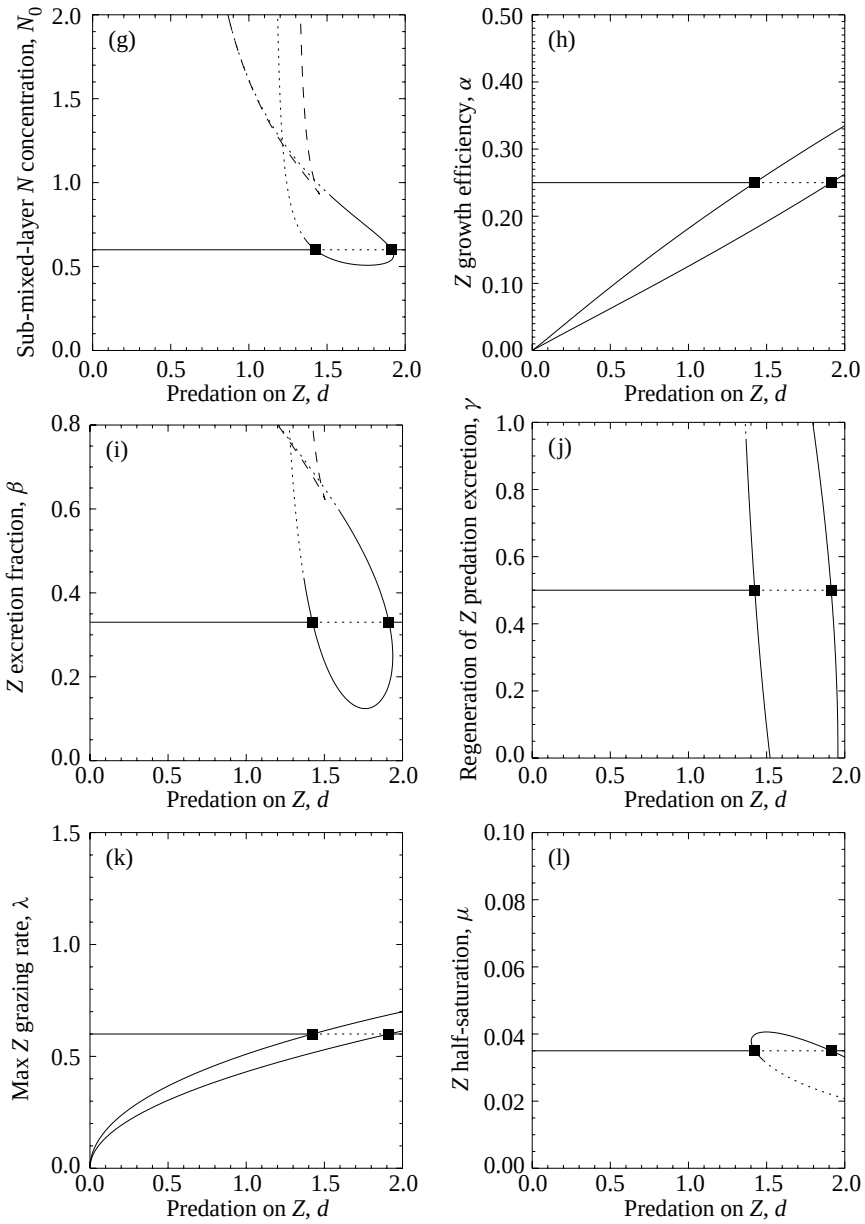

Figure 5. Continued

steady state (indicated by curves of long dashes)—we proved that such bifurcations, which result in multiple co-existing steady states, cannot occur for the linear case in the analysis of Section 3. These differences make the linear case diagrams appear altogether simpler than those for the quadratic case, and means that the variety of one-parameter bifurcations shown in Fig. 6 of EB96 will not occur for the linear case. These diagrams showed, at increasing fixed levels of N_0, branches

of unstable cycles arising from subcritical Hopf bifurcations and terminating at homoclinic connections to saddle points (which arose from fold bifurcations of the steady states). However, expecting the absence of such behaviour to imply that the limit-cycle behaviour will be simpler for the linear case than for the quadratic case turns out to be misguided, as will be demonstrated by the contours of constant period to be presented in Section 7. The absence of fold bifurcations in the linear case means that the Hopf bifurcation curves cannot cross over each other, because there are never co-existing steady states in the strictly positive octant.

7. Dependence of the Period of Oscillations on the Parameter Values

In Fig. 2(b) we showed that N, P and Z settle down to oscillations with a period of about 35 days when $q = 0.11$ and the other parameters are set to their default values. In Fig. 3(d) we then showed how the period changes as q is varied across the region of oscillations, i.e. between the two Hopf bifurcations. We now investigate how the period of the oscillations changes with respect to each of the other parameters in the model.

In Fig. 6 we plot contours (or isochrones) of constant period, within the regions of oscillatory behaviour given by Fig. 4. The contours are computed with the aid of LOCBIF, using a technique that we describe in the Appendix. The numbered curves are the contours, along which the period takes the constant value, in days, specified by the number. The key for the remaining features of these diagrams is the same as for Fig. 4. The range of q shown in each diagram is 0.075–0.15, as no oscillations occur for $q < 0.075$; (for the α and λ diagrams, oscillations do occur for $q < 0.075$, but at values below the minimum values of $\alpha = 0.2$ and $\lambda = 0.6$ given in Table 1). We plot contours at increments of 5 days, up to and including the 100-day contour (where applicable), and then show the 125, 150 and 175 contours, except for Fig. 6(a) for a/b where we show the 105, 110, 115 and 120 contours.

Figure 6(a) shows that an increase in a/b, due perhaps to increased sunlight, tends to decrease the period of the oscillations. Thus a higher maximum phytoplankton growth rate gives faster oscillations, as might be expected since the phytoplankton can respond to events more quickly. Figure 6(b) shows that the period tends to increase as the phytoplankton self-shading, c, increases. An increase in c reduces the phytoplankton growth term

$$\frac{N}{e+N}\frac{a}{b+cP}P,$$

and would be expected to have the same effect as a reduction in a/b. This is confirmed by the behaviour of the period, which increases as either c increases or a/b decreases. Similarly, increasing e reduces the growth term, and Fig. 6(c) shows that increasing e tends to increase the period (except at low e and q values).

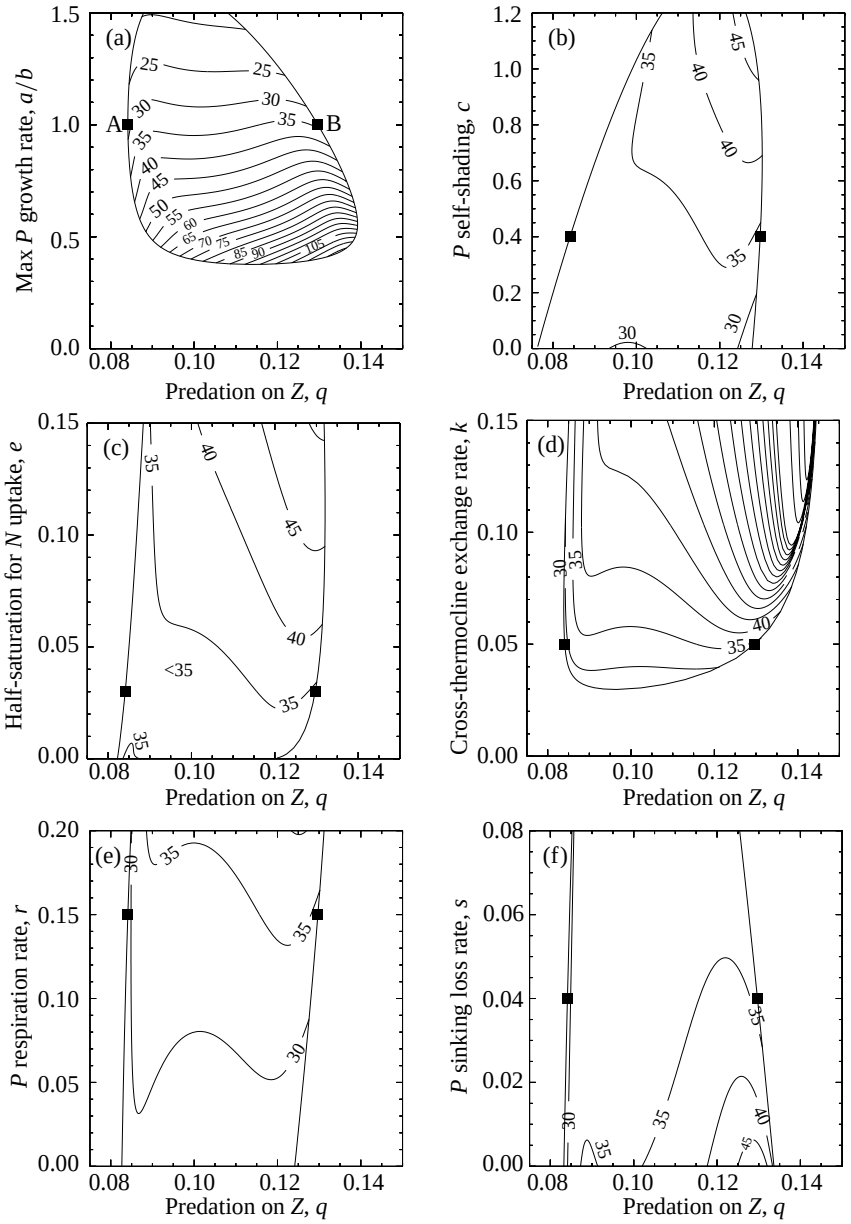

Figure 6. Within the regions of oscillations given by Fig. 4, the variations in period of the stable limit cycles are indicated by contours of constant period. The numbers indicate the period, in days, along contours, which are plotted at increments of 5 days up to 100 days, and then the 125, 150 and 175 contours are shown (except for a/b where we continue at five-day intervals). For k, N_0, β and μ, diagrams (d), (g), (i) and (l) respectively, period-doubling bifurcations occur; these are indicated by gaps in the contours (see text).

The diagrams for k, N_0 and β, Figs 6(d), (g) and (i), are very similar, with the β diagram being a stretched version of the other two diagrams. Contours of

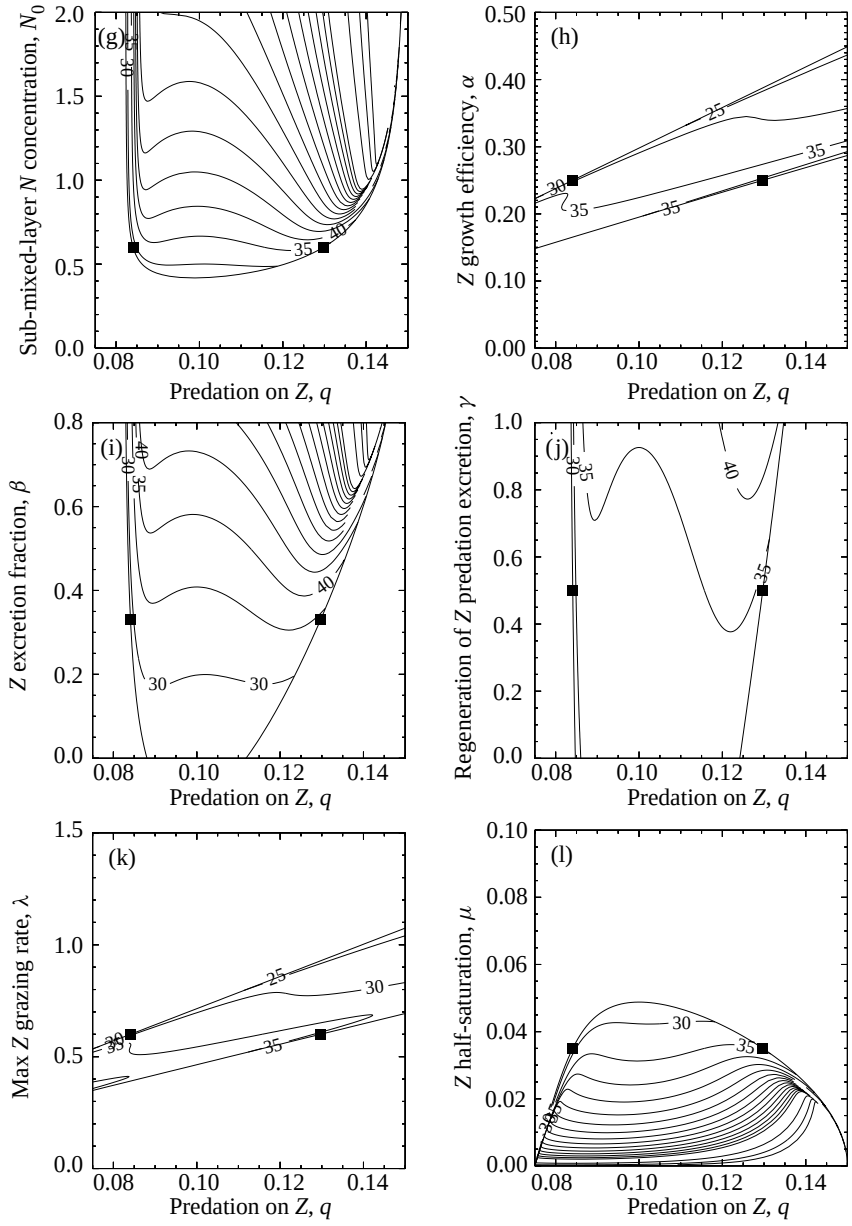

Figure 6. Continued

175 days are reached (we do not compute any higher values), and period-doubling bifurcations occur, which are shown by the gaps in some of the contours. The lowest contour for which a period-doubling bifurcation occurs for each of k, N_0 and β is the 55 contour. A period-doubled cycle resulting from such a bifurcation will then, by definition, have a period of 110 days, and will take the form of a

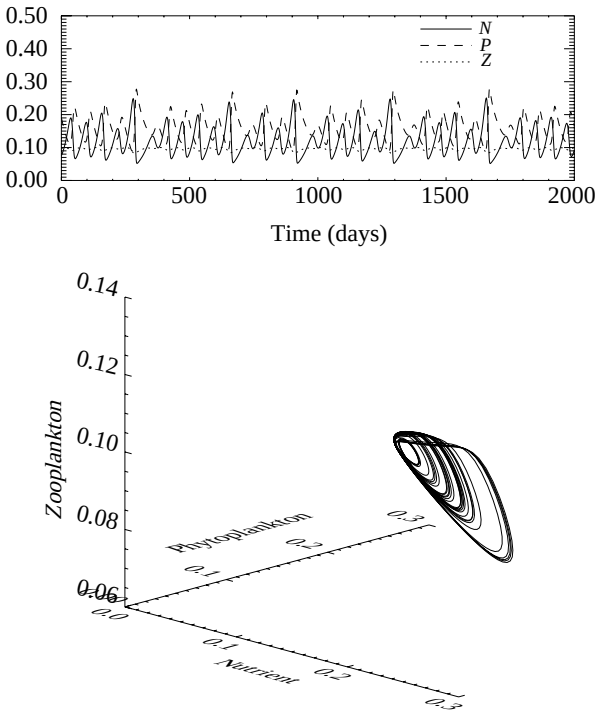

Figure 7. The time series and phase-space trajectory for $N_0 = 1.0$ and $q = 0.142$. The transient behaviour is not shown, and the trajectory is attracted onto an attractor which appears to be chaotic.

double-loop, with each 'loop' having a period of roughly 55 days. However, to try and illustrate the periods of the period-doubled cycles on the contour diagrams would lead to incomprehensibility rather than enlightenment, and so we leave the gaps in the contours to indicate where the original (undoubled) cycles are unstable.

Edwards (1997) showed that a cascade of period-doubling bifurcations occurs (as q increases) when N_0 is set to 1.0, resulting in an apparently chaotic attractor at $q = 0.142$, which we show in Fig. 7. For clarity the transient behaviour is not shown. For the N_0 bifurcation diagram, we additionally find fold bifurcations of cycles along the 150 and 175 contours [see Edwards (1997)]. As can be seen from the bifurcation diagrams, such regions where the original cycles that emanate from the Hopf bifurcations become unstable are relatively small, illustrating how rare chaotic attractors appear to be (since chaotic attractors most likely occur only in such regions). Indeed, a slight change in parameter values will destroy the attractor shown in Fig. 7. We have presented the attractor to complete the examples of the three basic attractors (steady state, limit cycle and chaotic attractor) exhibited by the model, but we emphasize the scarcity of chaotic behaviour. Note that we have not computed contours for periods greater than 175 days, and so some 'empty' regions in

the diagrams do actually contain stable cycles of large period—the period-doubled cycles only occur where there are gaps in the contours.

Figure 6(e) shows that the period increases as r is increased, whilst Fig. 6(f) shows that the period decreases as s is increased. Now, s is purely a linear loss of phytoplankton whilst r appears in the equations as both a linear phytoplankton loss and as a nutrient input. The bifurcation diagrams of Figs 4(e) and (f) (without the contours) for r and s are very similar, implying that r behaves more like s, as a phytoplankton loss, than as N_0, say, a nutrient input. But this is contradicted by the contour pictures—the period behaves more like N_0, increasing with increased r or N_0, even though the actual bifurcation picture is different. The increase in period for r is not as dramatic as that for N_0. Since the sensitivity of the period to s is actually quite weak, the consequence of an increase in r acting as a nutrient input is to pull the period up, overcoming the much weaker reduction due to its behaviour as a phytoplankton loss (like s). However, such interpretations should be treated with caution, because the actual loss is rP, and increasing r could actually cause rP, averaged over one cycle or taken at equilibrium, to decrease, a counter-intuitive but feasible notion. Figure 6(j) shows that the γ picture is similar to the r picture, which is consistent with the notion of r being considered more as a nutrient input.

Figures 6(h) and (k) show that α and λ have similar minor influences on the period, and that increasing the maximum zooplankton grazing rate, λ, has the opposite effect on the period to increasing the maximum phytoplankton growth rate, a/b. Finally, the μ diagram, Fig. 6(l), exhibits very high periods at low values of μ, plus period-doubling bifurcations on the contours from 50 upwards. Hopf A becomes subcritical at low values of q and μ, and μ is the only parameter for which we have found subcritical Hopf bifurcations in the linear case. However the consequences of this are fairly insignificant, and we will explain the effect of subcritical Hopf bifurcations more fully with regard to Fig. 8. The behaviour of the contours near to the region of period-doubling bifurcations is not quite as simple as for k, N_0 and β, since the Floquet multipliers undergo exotic excursions around the complex plane [described by Edwards (1997)].

In Fig. 8 we show the equivalent period-contour diagrams for the quadratic zooplankton mortality model, with d plotted from 1.0 to 2.0. Comparing Figs 6 and 8 for the linear and quadratic models, we find that, for each parameter, the general tendency of an increase in that parameter either to increase or decrease the period is the same for the two models. For example, Fig. 6(e) and Fig. 8(e) show that an increase in r will increase the period of the oscillations for both of the models.

The periods for the quadratic case attain narrower ranges of values than for the linear case, and only reach values above 55 days in Figs 8(d), (g) and (i) for k, N_0 and β, which we shall discuss shortly. However, note that the actual areas between the Hopf bifurcations for the quadratic case are smaller than those for the linear case, which may give less scope for a large range of periods to be reached. For the quadratic case we do not find period-doubling bifurcations along any of the

contours, in contrast to the linear case for which such bifurcations are the starting point for cascades of period-doubling bifurcations culminating in chaos.

The diagrams for k, N_0 and β, Figs 8(d), (g) and (i) respectively, are very similar, and we now explain Fig. 8(g) in detail. The contours are computed at intervals of 5 days up to the 100-day contour, and then the 125 contour is shown. There is no noticeable difference on the diagram between the (unlabelled) 100 and 125 contours. When the Hopf bifurcations are subcritical, as shown by the lines of short dashes in Fig. 8(g) and seen more clearly in the original Fig. 5(g), unstable cycles emanate from the Hopf bifurcations and can become stable at fold bifurcations. The point at which a Hopf bifurcation changes from being supercritical to subcritical is called a Bautin bifurcation (Kuznetsov, 1995), and from this a branch of fold bifurcations of limit cycles must emanate. In Fig. 8(g) a fold of a limit cycle is indicated by the termination of a contour, because we do not plot the contours for points where the cycles are unstable. Such terminations occur to the left of the curve of subcritical Hopf bifurcations. It is seen that the region of coexistence of stable limit cycles and stable steady states, which is bounded by the subcritical Hopf curve and the termination of the contours, is fairly small, and that the oscillations occur in a region which is only slightly larger than the region bounded by the Hopf bifurcation curves. On Fig. 6(l), the μ diagram for the linear case, the region of coexistence of a stable steady state with a stable limit cycle close to the subcritical Hopf bifurcation cannot clearly be seen, and is extremely narrow in size.

By plotting one-parameter diagrams of N against d, with N_0 held constant at various levels, Edwards (1997) determined that at some N_0 value between 1.25 and 1.35, the fold bifurcations of the limit cycles disappear, most likely by coming together at a cusp point (on a diagram of N_0 against d). For N_0 values above this cusp point no stable cycles exist, and hence no period contours are plotted. This cusp point is where the contours reach their maximum N_0 value on Fig. 8(g). Edwards (1997) presented the full bifurcation diagram of N_0 against d, adding curves of bifurcations of limit cycles to the steady-state bifurcations shown in Fig. 5(g).

Furthermore, Edwards (1997) showed that unstable cycles can terminate at homoclinic connections to saddle points. As a cycle approaches a homoclinic connection its period tends to infinity. Along a branch of cycles the period changes continuously, even through a fold bifurcation. This helps explain why we find stable cycles with relatively large period in the N_0 diagram. The diagrams for k, N_0 and β are the only ones for which we find fold bifurcations of steady states, and subsequent homoclinic behaviour, and these are the only diagrams exhibiting stable cycles with a period greater than 50 days.

No stable homoclinic orbits were detected, and Edwards (1997) used the Andronov–Leontovich theorem (Kuznetsov, 1995; Glendinning and Laing, 1996) to show that, almost certainly, no stable homoclinic orbits exist in the N_0 diagram. The Andronov–Leontovich theorem essentially states that the stability of a homoclinic orbit (and consequently the branch of cycles close to it in parameter space) is determined by the sum of the dominant eigenvalues of the associated saddle equi-

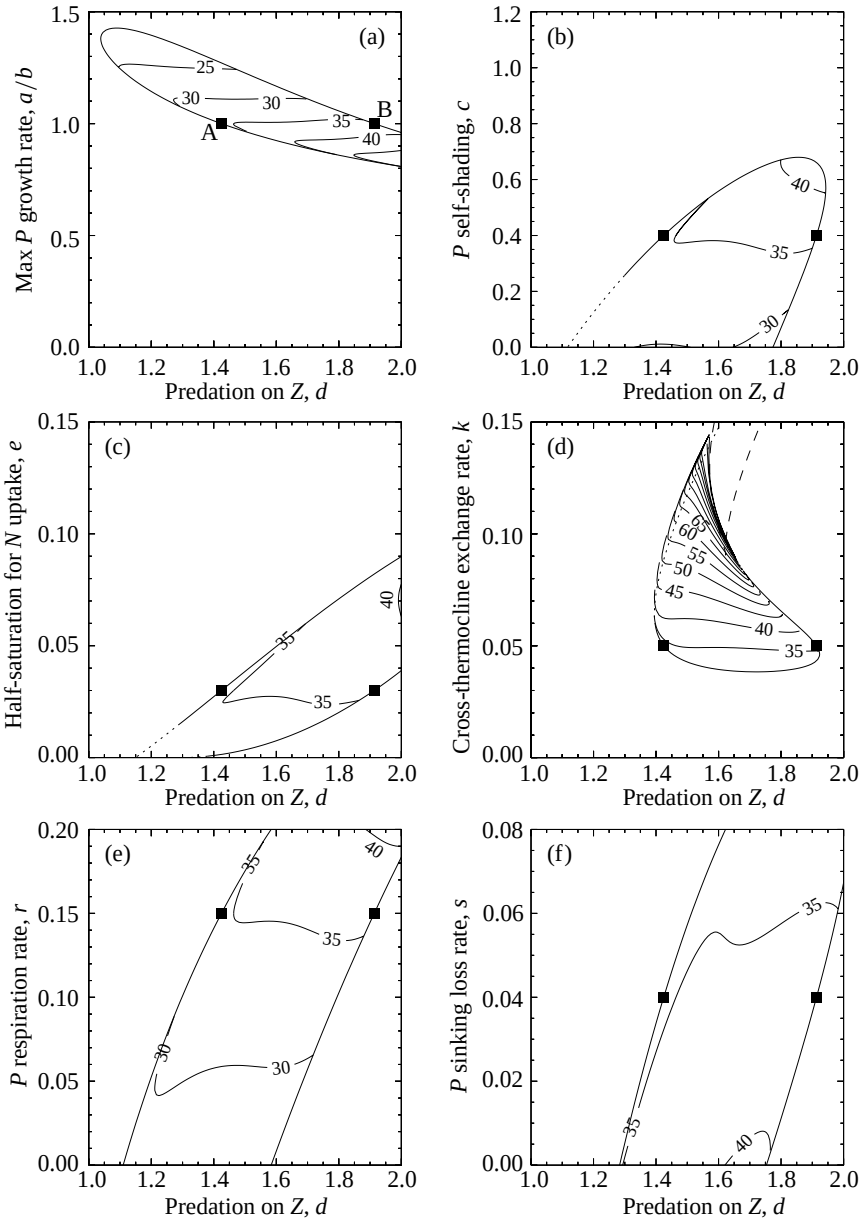

Figure 8. The steady-state bifurcation diagrams for the quadratic case are reproduced, and the variations in period of stable limit cycles are indicated by contours of constant period. The numbers indicate the period, in days, along each contour. Overall, we find less variation in the period than occurred for the linear case, with no period-doubling bifurcations (and no subsequent chaotic attractors).

librium point, where the dominant eigenvalues, when the eigenvalues are real, are the negative eigenvalue closest to zero and the positive eigenvalue closest to zero. Furthermore, the relevant saddle equilibrium points were always found to be saddle

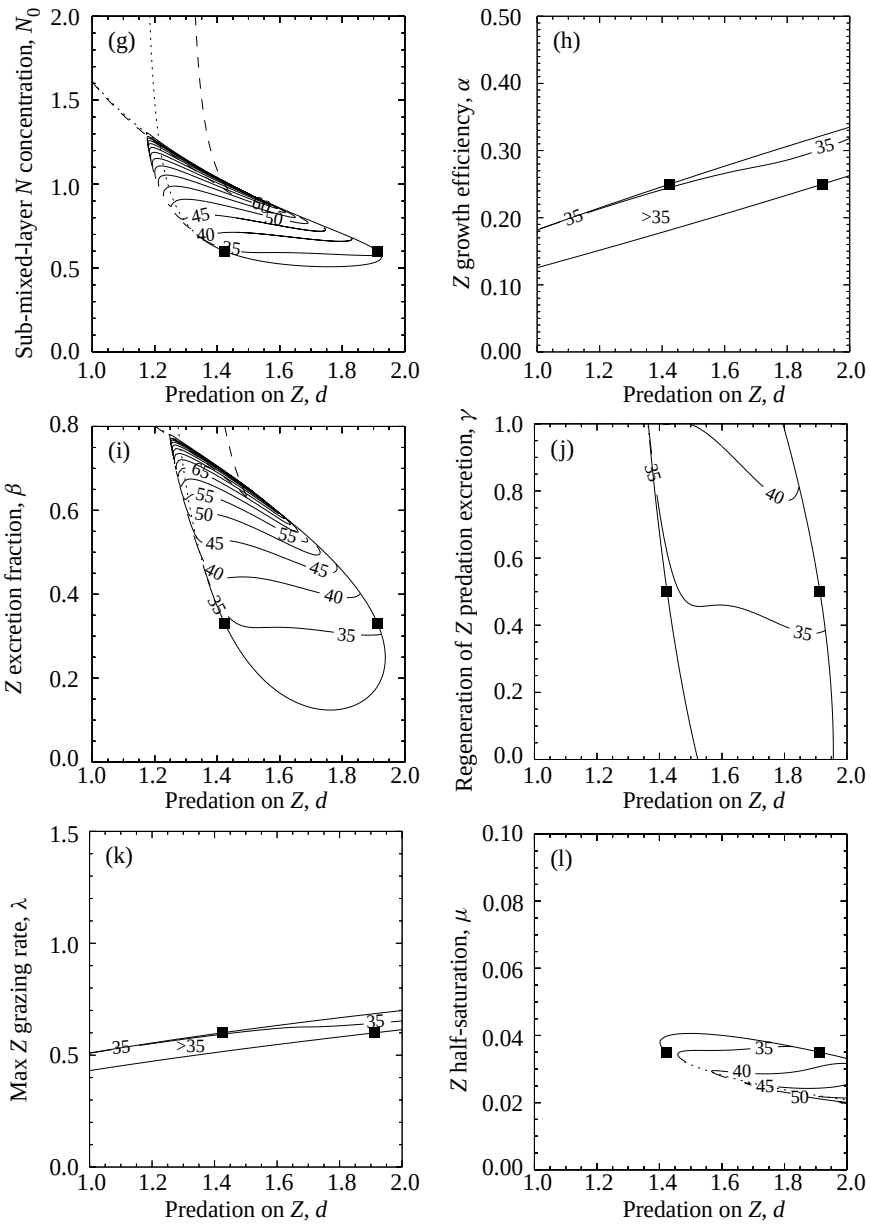

Figure 8. Continued

nodes, and did not become saddle foci. This means that we cannot have homoclinic orbits to a saddle focus (Glendinning and Sparrow, 1984; Mullin, 1993), and eliminates the possibility of multiple homoclinic orbits exhibiting period-doubling cascades to chaos.

So overall we find narrower ranges of periods for the quadratic case than for the linear case. Large periods are reached for the quadratic case only in the vicinity of

unstable homoclinic connections to saddle points. These saddle points arise from fold bifurcations of steady states, which are found only in the diagrams for k, N_0 and β. Except for these homoclinic cases, as parameters are independently varied the period is confined to roughly the range 25–50 days, only reaching 25 in one case and 50 in one other. For the linear case the diagrams for k, N_0 and β also exhibit large periods, even though no homoclinic connections exist.

8. DISCUSSION

We have investigated the behaviour of the three-component plankton model formulated by Edwards and Brindley (1996), but with linear, rather than quadratic, zooplankton mortality to represent different ecological assumptions. Our motivation came from the demonstration by Edwards and Brindley (1996) that unforced oscillations occur over broad regions of parameter space when the quadratic mortality term is used. This contrasts with the oft-quoted findings of Steele and Henderson (1992), who only found oscillations to occur when the linear term was used. In this paper, we have found that oscillations do indeed occur for the linear case, and that the regions of parameter space that exhibit oscillations are generally similar to the quadratic case. Oscillations appear to occur over a greater range of parameter values for the linear case than for the quadratic case, which is consistent with Steele and Henderson's simulations. It would have been surprising, given Steele and Henderson's results, if we had found oscillations to be more common for the quadratic case.

Yool (1998) analysed the full seven-component Fasham (1993) model, and found that unforced oscillations of the variables occurred when the cross-thermocline mixing rate and the sub-thermocline nutrient concentration were set to high values. These are equivalent to parameters k and N_0 in our models, and we too have found oscillations to occur only at high values of these parameters. Furthermore, Yool (1998) investigated the Fasham (1993) model with the linear and the quadratic mortality terms qZ and dZ^2, using our notation. [Note that Fasham and Yool refer to the linear and quadratic terms as 'constant' and 'linear' respectively, referring to the *specific* mortality rates q and dZ, and also note that Fasham originally used a hyperbolic mortality term, of the form $\sigma Z^2/(\theta+Z)$.] Yool set the cross-thermocline mixing rate to a high value, keeping all other parameters at Fasham's values, and varied q and d. He found unforced oscillations to occur as q varied, but not as d varied; this is analogous to our Figs 4(d) and 5(d). Yool's results do not preclude oscillations from occurring in the quadratic case, but show that our findings of oscillations being more common for the linear case could also hold for the much larger Fasham model, and hence may indeed be a general result applicable to many models.

The differing mortality functions that we have used change the definitions of the steady states, and for the linear case there is no possibility of coexisting steady

states with positive values of N, P and Z, in contrast to such coexistence found by Edwards and Brindley (1996) for the quadratic case. One objectionable consequence of the linear mortality term is that the phytoplankton steady-state value, P^*, depends only upon the parameters that appear in the zooplankton equation. Thus an increased nutrient input or a change in phytoplankton growth rate leaves P^* unaffected. Conversely, an undesirable aspect of the quadratic mortality term is that the zooplankton cannot die out unless the phytoplankton do, because the $({N_1}^*, {P_1}^*, 0)$ steady state cannot become stable.

One way of avoiding both of these problems, but which makes analytical work more intractable, is to use a combined form $qZ + dZ^2$. Such a form was used by McGillicuddy *et al.* (1995), although the actual values of q and d were 'tuned to maximize agreement between the model and available data'. Preliminary results by us show that with $q = 0.01$ and $d = 1.0$ (i.e., our default value of d with a small amount of linear mortality, q) the two-parameter bifurcation diagrams of Fig. 5 are essentially unchanged, with the Hopf bifurcations occurring at slightly lower values of d than for the default quadratic case. Analytically we find that the three-way transcritical bifurcation that occurs at $\Phi = 0$ for the quadratic case splits into two transcritical bifurcations (as for the linear case), illustrating that the three-way transcritical bifurcation is structurally unstable. The $qZ + dZ^2$ form could be interpreted as q representing natural mortality and d representing higher predation, thus removing the common assumption that the single forms qZ or dZ^2 model both types of mortality. We have not looked at the use of Holling-type functions, which saturate for large Z. These have been used in the higher-order models of Frost (1987), Hofmann and Ambler (1988) and Fasham (1993), but require estimation of an additional poorly known parameter (as does the $qZ + dZ^2$ form), an objection given by Steele and Henderson (1992).

The existence of a homoclinic connection would be sufficient to produce cycles with periods taking values up to infinity. So in the absence of any homoclinic connections for the linear case, it may have been expected that the high periods of limit cycles reached for the quadratic mortality case would not occur here. However, the period-contour diagrams show that high periods do indeed occur. Furthermore, we find period-doubling bifurcations, and subsequent cascades to chaos, whereas no such bifurcations or chaotic behaviour were found for the quadratic case. A question worth asking is whether the fact that we have found chaotic behaviour for the linear model, but not for the quadratic model, is due to the differences in the model structures. In other words, is there something fundamental that keeps a model with quadratic zooplankton mortality from exhibiting chaos?

Recent work by Caswell and Neubert (1998) shows that this is not true for the simple three-species food chain model of Hastings and Powell (1991). The Hastings and Powell model consists of a top predator, species Z, which feeds on intermediate species Y, which in turn feeds on basal species X. Species X undergoes logistic growth, the two feeding relationships are Holling type II functions, and the mortalities of species Y and Z are modelled with linear functions. Hastings and Powell

(1991) demonstrated the existence of a chaotic 'tea-cup' attractor. Caswell and Neubert (1998) show that if the aforementioned combined form $qZ + dZ^2$ replaces the linear function for mortality of the top predator, Z, then a chaotic tea-cup attractor can still occur. In particular, they present a chaotic attractor for $q = 0$, proving that solely quadratic mortality of the top predator does not exclude the possibility of chaos in three-species models in general.

Perhaps there does exist chaotic behaviour for our quadratic mortality model investigated in Edwards and Brindley (1996), but we have just not been in the right region of parameter space to observe it. However, we did not find any period-doubling bifurcations of limit cycles (these would have been detected during the construction of the period-contour diagrams in Section 7), and Edwards (1997) found that, in the relevant places, saddle points were saddle nodes and did not become saddle foci. This latter fact eliminates the possibility of multiple homoclinic orbits exhibiting period-doubling cascades to chaos [see Glendinning and Sparrow (1984), and Mullin (1993)], and the former finding means that we do not find a bifurcation to initiate a conventional period-doubling cascade of limit cycles. So, we do not even find the starting points for two routes to chaos, suggesting that if a region of chaos does occur, we are not close to it in parameter space.

We anticipate that our results, particularly the two-parameter bifurcation diagrams, should prove useful to modellers in interpreting the output of models. It is of interest to ascertain if the results apply to other models. Fasham *et al.* (1993) coupled the seven-component model of Fasham *et al.* (1990) to a general circulation model of the North Atlantic, and did not find any large-amplitude limit cycles. However, they noted that Toggweiler (1990) used the same ecosystem model and did observe such cycles for high nitrate input conditions corresponding to the Peruvian upwelling region of the Pacific. High nitrate input in our models is given by high values of the cross-thermocline exchange rate, k, or the sub-mixed-layer nutrient concentration N_0. For both of our models, the corresponding two-parameter bifurcation diagrams indicate that limit cycles do not occur at low values of these parameters but can at higher values, in accord with the comments of Fasham *et al.* (1993).

We have investigated our models under constant summertime physical conditions, assuming a constant mixed-layer depth and constant incident radiation. The periods of oscillations that we have found are consistent with those found in freshwater plankton populations (McCauley and Murdoch, 1987), where physical conditions are more stable than in the ocean, and with periods that occur during the summer in the large ocean ecosystem model of Fasham (1993). However, our global approach of varying all the parameters and computing the periods in Figs 6 and 8 demonstrates that the models are capable of producing oscillations with a whole range of periods. We have run simulations with a forced mixed-layer depth (Edwards, 1997), and shown how the analytical and numerical results presented here can explain all the features of the annual cycle, including the absence or presence of spring blooms and oscillations in the summer. Edwards (1997) has also added a fourth component, explicitly modelling detritus, to our *NPZ* model, showing that such a change to the

structure of the model actually has less of an effect on the behaviour than do the alternative zooplankton mortality terms. This shall be reported elsewhere.

Our work applies the powerful mathematical theory of dynamical systems to the area of plankton population modelling, and improves our understanding of the dynamics of simple models. This approach has allowed us to examine the behaviour of models across wide ranges of all parameters—usually modellers only investigate the consequences of varying a few parameters. Our two-parameter bifurcation diagrams, indicating how oscillations persist across parameter space, allow us to compare the models in a more complete way than the traditional approach of multiple simulations. Fasham (1993) discussed whether one generic plankton model can be constructed that would be sufficient to model all the areas of the world's oceans. At present this question remains unanswered. The results presented here improve the understanding of the dynamics of plankton models, and we hope that they will play a small part towards future development of models, possibly culminating with such a generic model.

ACKNOWLEDGEMENTS

This work benefited from discussions with Andrew Yool, David Broomhead, Trevor Platt, Shubha Sathyendranath, and the members of Hal Caswell's mathematical ecology group at Woods Hole. We also thank an anonymous referee for helpful comments. A.M. Edwards is grateful for financial support from: the William Wright Smith Scholarship, which funded postgraduate studies at the University of Leeds; ONR Grant Number N00014-92-J-1527 to Hal Caswell, plus the Marine Policy Center of the Woods Hole Oceanographic Institution, which both funded postdoctoral work; and the Cambridge Philosophical Society for assistance in attending the *Mathematical Modelling of Plankton Population Dynamics* symposium at the Isaac Newton Institute in Cambridge, where many of the aforementioned discussions took place. This is WHOI Contribution No. 9721.

APPENDIX: USING LOCBIF TO COMPUTE CONTOURS OF CONSTANT PERIOD OF LIMIT CYCLES.

The period-contour diagrams of Figs 6 and 8 are computed using the interactive bifurcation software LOCBIF (Khibnik *et al.*, 1992, 1993). When following a branch of limit cycles, the period is treated as a parameter. Two parameters need to be allowed to vary in order to trace a branch, and these two parameters may or may not include the period, depending on whether or not a contour of constant period is required. The ease with which LOCBIF allows selection and deselection of active (varying) parameters is exploited to compute contours and find starting points for them. Consider Fig. 8 for the quadratic case. For the default parameter values an

orbit of 35 days occurs when $d = 1.46$; this orbit is used as the starting point in each diagram. Figure 3(d) of EB96 [which is similar to Fig. 3(d) here] suggests that, for each parameter, a 35 contour should exist close to the default value of the parameter across most of the range of d. Consider firstly Fig. 8(a), the diagram for a/b, which shows contours of 25, 30, 35, 40 and 45 days (the 45 contour is not labelled due to its short length). The 35 contour is computed first. Starting from the orbit at $d = 1.46$, the period is held fixed at 35 days and a/b and d are active (allowed to vary), so that the 35 contour is traced out in each direction. The contour terminates at each end at the Hopf bifurcation curve, i.e., the limit cycle being traced collapses onto the steady state. To then find the starting point for, say, the 30 contour, the original period-35 orbit at $d = 1.46$ is selected, and d is held fixed and a/b and the period are made active. As a/b increases, the period decreases until it reaches 30, and this point is used as the starting point of the 30 contour.

This process is repeated to find the starting point of the 25 contour, and a similar method used to find starting points for the other contours. During the searching process, the edge of the oscillatory region (i.e., the Hopf bifurcation curve) may be reached before the period reaches the next required value. This occurs, for example, when starting from $d = 1.46$ on the 35 contour and decreasing a/b in order to find a period-40 orbit to start the 40 contour. This is overcome by simply fixing a/b at a point just above the Hopf curve, and then increasing d until a period-40 orbit is reached. Thus, extending this process, by keeping one of the two parameters fixed we can trace along limit cycle branches by moving vertically and horizontally through the oscillatory region until each required period is reached. Moving horizontally, with a/b fixed, and d and the period varying, is just what we did in Fig. 3(d) of EB96 [and Fig. 3(d) here with q varying] when a/b was fixed at its default value.

We now show that no contours of 20 days can start from the Hopf bifurcation curve in the a/b diagram. By definition, two of the eigenvalues of the Jacobian of the steady state at a Hopf bifurcation exist as a complex and conjugate pair with zero real part, which we denote as $\pm\omega i$. The period of a limit cycle which emanates from a Hopf bifurcation is then given, sufficiently close to the Hopf bifurcation, by $2\pi/\omega$ [see, for example, page 272 of Wiggins (1990)]. The contour of 35 days therefore terminates on the Hopf bifurcation curve at (or at least arbitrarily close to) the locations where $\omega = 2\pi/35$. Thus, by noting the values of ω as we move along the Hopf bifurcation curves we can determine, prior to actually calculating any limit cycles, where the contours will terminate, and what the minimum and maximum contours which terminate on the Hopf bifurcation curve will be. For the a/b curve, the maximum value of ω is 0.303, corresponding to a minimum period of 20.7 days, and is reached on the upper-left portion of the curve. This does not quite guarantee that no 20 contours will exist at all, since a contour could form an isolated closed loop (inside which the period is less than 20). But this seems unlikely given the decreasing nature of the period as we move towards the upper-left point of the oscillatory region. Indeed, tracing limit cycles by moving horizontally

and vertically through the upper-left region we do not find any orbits with a period of 20 days, virtually verifying that no closed-loop 20 contours exist.

LOCBIF computes the Floquet multipliers of limit cycles, and detects local bifurcations of limit cycles such as fold, period-doubling or Naimark–Sacker bifurcations. No such bifurcations are found along any of the contours in Fig. 8(a) (and hence the limit cycles are always stable), or indeed in the quadratic-case diagrams for any of the parameters except for k, N_0, β and μ, for which fold bifurcations occur; in these diagrams the contours only represent the period of stable orbits.

For the linear case, we do find period-doubling bifurcations of limit cycles. As a contour is traced out, if a period-doubling bifurcation is reached (i.e., a Floquet multiplier leaves the unit circle through -1), then we continue computation of the contour, but do not plot it when the cycles in question are unstable (i.e., whilst the Floquet multiplier remains outside of the unit circle). In most cases we find that the cycles then restabilize at a second period-doubling bifurcation (i.e., the Floquet multiplier re-enters the unit circle through -1), and the remainder of the contour corresponds to stable cycles, and is thus plotted. We find that period-doubling bifurcations only occur for k, N_0, β and μ, Figs 6(d), (g), (i) and (l) respectively. So in these diagrams we see small regions of gaps in some of the contours, the edges of these regions indicating the locations of the period-doubling bifurcations. These occur at high q values in each picture, and are most clearly seen in Fig. 6(i) for β.

REFERENCES

Adams, J. A. and J. H. Steele (1966). Shipboard experiments on the feeding of *Calanus finmarchicus* (Gunnerus), in *Some Contemporary Studies in Marine Science*, H. Barnes (Ed), London: George Allen and Unwin, pp. 19–35.

Armstrong, R. A. (1994). Grazing limitation and nutrient limitation in marine ecosystems: Steady state solutions of an ecosystem model with multiple food chains. *Limnol. Oceanogr.* **39**, 597–608.

Caswell, H. and M. G. Neubert (1998). Chaos and closure terms in plankton food chain models. *J. Plankton Res.* **20**, 1837–1845.

Collie, J. S. and P. D. Spencer (1994). Modeling predator–prey dynamics in a fluctuating environment. *Can. J. Fish. Aquat. Sci.* **51**, 2665–2672.

Denman, K., E. Hofmann and H. Marchant (1996). Marine biotic responses to environmental change and feedbacks to climate, in *Climate Change 1995 - The Science of Climate Change. Contribution of Working Group I to the Second Assessment Report of the Intergovernmental Panel on Climate Change*, J. T. Houghton, L. G. Meira-Filho, B. A. Callander, N. Harris, A. Kattenberg, and K. Maskell, (Eds), Cambridge: Cambridge University Press, pp. 482–516.

Doedel, E., X. Wang and T. Fairgrieve (1994). AUTO: Software for continuation and bifurcation problems in ordinary differential equations, Applied Mathematics Report, CA: California Institute of Technology.

Edwards, A. M. (1997). A rational dynamical-systems approach to plankton population modelling, PhD thesis, University of Leeds, U.K.

Edwards, A. M. and J. Brindley (1996). Oscillatory behaviour in a three-component plankton population model. *Dyn. Stab. Syst.* **11**, 347–370.

Evans, G. T. and J. S. Parslow (1985). A model of annual plankton cycles. *Biol. Oceanogr.* **3**, 327–347.

Fasham, M. J. R. (1993). Modelling the marine biota, in *The Global Carbon Cycle*, M. Heimann (Ed), Berlin: Springer-Verlag, pp. 457–504.

Fasham, M. J. R., H. W. Ducklow and S. M. McKelvie (1990). A nitrogen-based model of plankton dynamics in the oceanic mixed layer. *J. Mar. Res.* **48**, 591–639.

Fasham, M. J. R., J. L. Sarmiento, R. D. Slater, H. W. Ducklow and R. Williams (1993). Ecosystem behavior at Bermuda Station "S" and Ocean Weather Station "India": a general circulation model and observational analysis. *Glob. Biogeochem. Cyc.* **7**, 379–415.

Frost, B. W. (1987). Grazing control of phytoplankton stock in the open subarctic Pacific Ocean: a model assessing the role of mesozooplankton, particularly the large calanoid copepods *Neocalanus* spp. *Mar. Ecol. Prog. Ser.* **39**, 49–68.

Glendinning, P. (1994). *Stability, Instability and Chaos: An Introduction to the Theory of Nonlinear Differential Equations*. Cambridge Texts in Applied Mathematics, Cambridge: Cambridge University Press.

Glendinning, P. and C. Laing (1996). A homoclinic hierarchy. *Phys. Lett. A* **211**, 155–160.

Glendinning, P. and C. Sparrow (1984). Local and global behavior near homoclinic orbits. *J. Stat. Phys.* **35**, 645–696.

Guckenheimer, J. and P. Holmes (1983). *Nonlinear Oscillations, Dynamical Systems, and Bifurcations of Vector Fields*, Vol. 42 of *Applied Mathematical Sciences*, New York: Springer-Verlag.

Hastings, A. and T. Powell (1991). Chaos in a three-species food chain. *Ecology* **72**, 896–903.

Henderson, E. W. and J. H. Steele (1995). Comparing models and observations of shelf plankton. *J. Plankton Res.* **17**, 1679–1692.

Hofmann, E. E. and J. W. Ambler (1988). Plankton dynamics on the outer southeastern U.S. continental shelf. Part II: A time-dependent biological model. *J. Mar. Res.* **46**, 883–917.

Khibnik, A. I., Y. A. Kuznetsov, V. V. Levitin and E. V. Nikolaev (1992). Interactive LOCal BIFurcation analyzer. Computer Algebra Netherlands.

Khibnik, A. I., Y. A. Kuznetsov, V. V. Levitin and E. V. Nikolaev (1993). Continuation techniques and interactive software for bifurcation analysis of ODEs and iterated maps. *Physica D* **62**, 360–371.

Kuznetsov, Y. A. (1995). *Elements of Applied Bifurcation Theory*, Vol. 112 of *Applied Mathematical Sciences*. New York: Springer-Verlag.

McCauley, E. and W. W. Murdoch (1987). Cyclic and stable populations: plankton as paradigm. *Am. Nat.* **129**, 97–121.

McGillicuddy, D. J., J. J. McCarthy and A. R. Robinson (1995). Coupled physical and biological modeling of the spring bloom in the North Atlantic (I): model formulation and one dimensional bloom process. *Deep-Sea Res. I* **42**, 1313–1357.

Mullin, T. (1993). A multiple bifurcation point as an organizing centre for chaos, in *The Nature of Chaos*, T. Mullin (Ed), Oxford: Oxford University Press, pp.51–68.

Nybakken, J. W. (1982). *Marine Biology: An Ecological Approach*. New York: Harper and Row.

Platt, T. and S. Sathyendranath (1993). Estimators of primary production for interpretation of remotely sensed data on ocean color. *J. Geophys. Res.* **98**, 14561–14576.

Platt, T., S. Sathyendranath and P. Ravindran (1990). Primary production by phytoplankton: analytic solutions for daily rates per unit area of water surface. *Proc. R. Soc. Lond., Ser. B*, **241**, 101–111.

Ryabchenko, V. A., M. J. R. Fasham, B. A. Kagan and E. E. Popova (1997). What causes short-term oscillations in ecosystem models of the ocean mixed layer? *J. Mar. Syst.* **13**, 33–50.

Steele, J. H. (1962). Environmental control of photosynthesis in the sea. *Limnol. Oceanogr.* **7**, 137–150.

Steele, J. H. and B. W. Frost (1977). The structure of plankton communities. *Phil. Trans. R. Soc. Lond., Ser. B*, **280**, 485–534.

Steele, J. H. and E. W. Henderson (1981). A simple plankton model. *Am. Nat.* **117**, 676–691.

Steele, J. H. and E. W. Henderson (1992). The role of predation in plankton models. *J. Plankton Res.* **14**, 157–172.

Steele, J. H. and E. W. Henderson (1993). The significance of interannual variability, in *Towards a Model of Ocean Biogeochemical Processes*, G. T. Evans and M. J. R. Fasham, (Eds), Berlin: Springer-Verlag, pp. 237–260.

Tait, R. V. (1981). *Elements of Marine Ecology - Third Edition*. London: Butterworths.

Taylor, A. H. and I. Joint (1990). A steady-state analysis of the 'microbial loop' in stratified systems. *Mar. Ecol. Prog. Ser.* **59**, 1–17.

Thompson, J. M. T. and H. B. Stewart (1986). *Nonlinear Dynamics and Chaos*, Chichester: John Wiley and Sons.

Thurman, H. V. (1997). *Introductory Oceanography*, 8th edition, Englewood Cliffs, NJ: Prentice-Hall.

Toggweiler, J. R. (1990). Modeling workshop offers first look at new simulation of Equatorial Pacific. *U.S. JGOFS News* **2**, 1 and 11.

Truscott, J. E. and J. Brindley (1994). Equilibria, stability and excitability in a general class of plankton population models. *Phil. Trans. R. Soc. Lond., Ser. A*, **347**, 703–718.

Wiggins, S. (1988). *Global Bifurcations and Chaos: Analytical Methods*, Vol. 73 of *Applied Mathematical Sciences*. New York: Springer-Verlag.

Wiggins, S. (1990). *Introduction to Applied Nonlinear Dynamical Systems and Chaos*, Vol. 2 of *Texts in Applied Mathematics*, New York: Springer-Verlag.

Williams, R. (1988). Spatial heterogeneity and niche differentiation in oceanic zooplankton. In G. A. Boxshall and H. K. Schimke, (Eds), *Biology of Copepods*. *Hydrobiologia* **167/168**, 151–159.

Wroblewski, J. S. (1989). A model of the spring bloom in the North Atlantic and its impact on ocean optics. *Limnol. Oceanogr.* **34**, 1563–1571.

Yool, A. (1998). The dynamics of open-ocean plankton ecosystem models, PhD thesis, University of Warwick, U.K.

Received 28 June 1998 and accepted 26 October 1998